Selecting Improved Peptidyl Motifs for Cytosolic Delivery of Disparate Protein and Nanoparticle Materials

Kelly Boeneman,[†,+] James B. Delehanty,[†,+] Juan B. Blanco-Canosa,[§,○,+] Kimihiro Susumu,[‡,#] Michael H. Stewart,[‡] Eunkeu Oh,[‡,#] Alan L. Huston,[‡] Glyn Dawson,[⊥] Sampat Ingale,[§] Ryan Walters,[⊥,∥] Miriam Domowicz,[⊥] Jeffrey R. Deschamps,[†] W. Russ Algar,[†,▽,◇] Stassi DiMaggio,[⊗] Janet Manono,[⊗] Christopher M. Spillmann,[†] Darren Thompson,[§] Travis L. Jennings,[◆] Philip E. Dawson,[§,*] and Igor L. Medintz[†,*]

[†]Center for Bio/Molecular Science and Engineering, Code 6900, [‡]Optical Sciences Division, Code 5611, U.S. Naval Research Laboratory, Washington, D.C. 20375, United States, [§]Departments of Cell Biology & Chemistry, The Scripps Research Institute, La Jolla, California 92037, United States, [⊥]Departments of Pediatrics, Biochemistry and Molecular Biology, [∥]Committee on Neurobiology, University of Chicago, Chicago, Illinois 60637, United States, [#]Sotera Defense Solutions, Annapolis Junction, Maryland 20701, United States, [▽]College of Science, George Mason University, Fairfax, Virginia 22030, United States, [⊗]Department of Chemistry, Xavier University of Louisiana, New Orleans, Louisiana 70125, United States, [○]Institute for Research in Biomedicine (IRB Barcelona), Chemistry and Molecular Pharmacology Programme, Barcelona 08028, Spain, and [◆]eBioscience, Inc., 10255 Science Center Drive, San Diego, California 92121, United States. [+]Authors contributed equally. [◇]Present address: Department of Chemistry, University of British Columbia, Vancouver, BC, V6T 1Z1 Canada.

ABSTRACT Cell penetrating peptides facilitate efficient intracellular uptake of diverse materials ranging from small contrast agents to larger proteins and nanoparticles. However, a significant impediment remains in the subsequent compartmentalization/endosomal sequestration of most of these cargoes. Previous functional screening suggested that a modular peptide originally designed to deliver palmitoyl-protein thioesterase inhibitors to neurons could mediate endosomal escape in cultured cells. Here, we detail properties relevant to this peptide's ability to mediate cytosolic delivery of quantum dots (QDs) to a wide range of cell-types, brain tissue culture and a developing chick embryo in a remarkably nontoxic manner. The peptide further facilitated efficient endosomal escape of large proteins, dendrimers and other nanoparticle materials. We undertook an iterative structure—activity relationship analysis of the peptide by discretely modifying key components including length, charge, fatty acid content and their order using a comparative, semiquantitative assay. This approach allowed us to define the key motifs required for endosomal escape, to select more efficient escape sequences, along with unexpectedly identifying a sequence modified by one methylene group that specifically targeted QDs to cellular membranes. We interpret our results within a model of peptide function and highlight implications for *in vivo* labeling and nanoparticle-mediated drug delivery by using different peptides to co-deliver cargoes to cells and engage in multifunctional labeling.

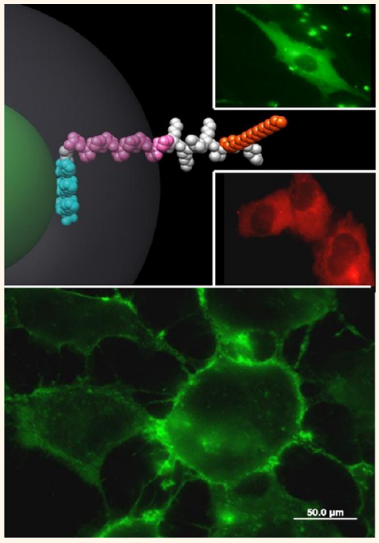

KEYWORDS: endosomal escape · cytosol · nanoparticle · quantum dot · peptide · fusogenic · cellular labeling · protein · cargo · dendrimer · membrane · cell penetrating peptide

Utilization of the HIV TAT (transactivator of transcription) polyarginine-basic motif, along with other sequences including penetratin, transportan, and Chariot/Pep-1 as cell penetrating peptides (CPPs) to deliver exogenous materials to cells has helped revolutionize cellular biotechnology.[1−8] In contrast to utilizing lipid polymers or electroporation, peptide-mediated delivery is attractive as peptides are small, easily synthesized, biocompatible and can be chemically linked to almost any molecule of interest. The exact mechanism of TAT-delivery has been contentious, with evidence presented for both endosomal uptake and a direct membrane translocation process. Current thinking suggests both possibilities, with the exact modality dependent on a complex interplay between cell-line, peptide sequence, physicochemical "cargo" properties and a host of other factors that are not fully understood.[2−5] Regardless, a nearly indescribable number of "cargoes"

* Address correspondence to Dawson@scripps.edu, Igor.medintz@nrl.navy.mil.

Received for review December 3, 2012 and accepted May 7, 2013.

Published online May 28, 2013
10.1021/nn400702r

including drugs, contrast agents, nucleic acids, proteins/antibodies, other peptides, nanoparticles, and synthetic polymers have undergone cellular delivery using TAT or related sequences.[1−5,9] With limited exceptions for some nucleic acids and highly lipophilic molecules, the vast majority of materials delivered to cells in this manner remain sequestered in the vesicular/endolysosomal system and never achieve full cytosolic access.[1,2,10] Endoosmolytic agents such as chloroquine or proton sponge polymers are available; however, they are generally toxic and of limited utility.[11,12] Endosomal escape or "fusogenic" peptides have also been reported, but have not proven robust for use with many different cargo types.[1,13] Although tumor specific peptides are a major interest for targeted chemotherapeutic nanomedicine, a critical need still remains for unique peptide sequences that are cumulatively capable of broadly mediating: (1) cellular uptake, (2) endosomal escape to the cytosol, (3) delivery of disparate cargoes ranging from small drugs to large nanoparticles, (4) delivery to a wide range of cells/tissues, and (5) accomplishing all this in a noncytotoxic manner.[1,2] This is especially relevant within the developing fields of theranostics and nanoparticle-mediated drug delivery.

We previously evaluated several proposed protocols for achieving cellular delivery and endosomal escape of semiconductor quantum dots (QDs).[11] Strategies tested included active protocols such as electroporation and nucleofection along with facilitated methods such as polymer- and peptide-mediated uptake. Promising results were noted with a modular peptide designed for the delivery of palmitoyl-protein thioesterase 1 (PPT1) inhibitors to neurons; these act as pharmacological chaperones in infantile Batten disease.[10,13] This parent peptide (see JB577, Table 1) consists of the sequence WG•(Dap^{Pal})•VKIKK•P_9•GG•H_6 and can be subdivided into functional modules as indicated by the breaks (•) in the sequence (see also Figure 6A). The core is (Dap^{Pal})•VKIKK, where *Pal* is a palmitoyl group anchored to a synthetic diaminopropionic acid (Dap) residue by a nonhydrolyzable amide linkage. VKIKK originates from the carboxy-terminal C^{Pal}VKIKK motif of the K-Ras4A signaling protein where it is recognized by palmitoyl transferases resident in the endoplasmic reticulum (ER)-Golgi. These catalyze cysteine palmitoylation *via* a hydrolyzable thioester linkage.[14−16] This post-translational modification, along with a related farnesylation, allows the K-Ras4A C-terminus to insert into the cell membrane where it participates in assembling the Ras-phosphorylation cascade.[15−17] Intracellularly, *Pal* thioester-attachment is reversed by PPT as part of the mechanism that controls Ras cellular localization.[14−16] The peptide's terminal His_6-module provides self-assembly to QDs *via* metal-affinity coordination as described[18,19] while the Pro_9 is thought to assume a type II helix providing a rigid spacer between the QD/His_6-attachment point and the peptide core. Finally, Gly_2 acts as a flexible hinge between the previous modules while Trp allows for spectroscopic quantitation. Poly(L-proline), polyhistidine and secondary amphipathic peptides displaying multiple Trp residues have been reported as efficient CPPs in their own right, making it unclear which elements of the sequence facilitate cytosolic delivery.[20−22] Preliminary screening of this peptide for QD cellular delivery indicated it could mediate rapid endocytic uptake of the QDs (1−2 h) followed by a slower cytosolic release that peaked ∼48 h after delivery.[11]

Here, we extensively characterize JB577 properties relevant to cytosolic delivery of QDs and demonstrate applicability to other cell-lines/model tissues. We show that JB577 also facilitates efficient cytosolic delivery of proteins, a dendrimer and other types of nanoparticles. We undertook an iterative structure−activity relationship (SAR) analysis[23−25] of the peptide to elucidate residues required for endosomal escape by modifying key motifs including charge, length, fatty acid content and domain order (Table 1). These analogues were evaluated within a comparative, semiquantitative assay, allowing us to select sequences demonstrating more efficient delivery along with one that delivers QDs specifically to cellular membranes (Table 2). The combinatorial application of peptides is highlighted by performing simultaneous multicolor QD cellular labeling.

RESULTS

Quantum Dots and Peptide Conjugation. Experiments primarily utilized green-550 nm or red-625 nm emitting CdSe/ZnS core/shell QDs solubilized with polyethylene glycol-modified dihydrolipoic acid (DHLA-PEG) or zwitterionic CL4-surface ligands; hydrodynamic diameter (H_D) ∼11.5 and ∼13 nm for 550-PEG and 625-CL4 QDs, respectively (chemical structures of the ligands are shown in the Supporting Information).[26] These ligands provide bright, stable nanocrystals that are nonfouling and soluble across a broad pH/ionic range. For peptide conjugation, we primarily utilized polyhistidine (His_n) metal-affinity coordination to the Zn-rich QD surface. This simple, high affinity (K_d ∼1 nM) self-assembly approach rapidly provides spontaneously-formed stoichiometric conjugates (sec to min) without requiring subsequent purification.[18] All peptides (Table 1) were synthesized as described in the Supporting Information. Prior physicochemical characterization studies suggested that ∼50 ± 10 peptides could be displayed on 530−550 nm QDs (diameter ∼6−6.5 nm) functionalized with DHLA-based ligands.[27] The larger diameter of the 625 nm QDs (∼10 nm) suggest a capacity to display a higher peptide valence.[28]

Characterization of Endosomal Escape. As an initial baseline, we confirmed our previous JB577 results in direct comparison to uptake mediated by the ubiquitous

TABLE 1. Peptides used in this study[a]

Peptide	Focus	Sequence	Description	Mw / charge pH 7.4
JB577	Parent	WGDap_aVKIKKP$_9$GGH$_6$	Parent peptide	3034 / +3
CS56 Pal-2	Pro$_n$-linker	WGDap_aVKIKKGLA$_4$GGH$_6$	Pro$_9$ → Ala$_4$	2615 / +3
CS56 Pal-3	Pro$_n$-linker	WGDap_aVKIKKGLAPAAGGH$_6$	Pro$_9$ → PAA	2641 / +3
JB582	Pro$_n$-linker	WGDap_aVKIKKP$_4$GGH$_6$	Pro$_9$ → Pro$_4$	2549 / +3
JB747	Pro$_n$-linker	WGDap_aVKIKKAib$_9$GGH$_6$	Pro$_9$ → Aib$_9$	2926 / +3
JB865	Pro$_n$-linker	WGDap_aVKIKKP$_{12}$GGH$_6$	Pro$_9$ → Pro$_{12}$	3326 / +3
JB864	Pro$_n$-linker	WGDap_aVKIKKP$_{15}$GGH$_6$	Pro$_9$ → Pro$_{15}$	3618 / +3
JB833	Pro$_n$/ Charge	WGDap_aAGAGGA$_4$AibA$_4$GGH$_6$	Uncharged /palm-only	2530 / 0
JB578	Charge	WGDap_aP$_9$GGH$_6$	No VKIKK – uncharged	2438 / 0
JB583	Charge	WGDap_aVRRRIRRP$_9$GGH$_6$	Lys → Arg	3431 / +5
JB585	Charge	WGDapVRRRIRRP$_9$GGH$_6$	No palmitoyl/Lys → Arg	3192 / +6
JB868	Charge	WGDapVRLP$_3$VRLP$_3$VRLP$_3$GGH$_6$	No palm /amphipathic-[VRLP$_3$]$_3$	3304 / +4
JB869	Charge	WGDap_aVRLP$_3$VRLP$_3$VRLP$_3$GGH$_6$	VKIKKP$_9$ → amphipathic-[VRLP$_3$]$_3$	3543 / +3
JB895	Charge	WGVKIKKDap_aVKIKKP$_9$GGH$_6$	2 x VKIKK	3633 / +6
JB579	Fatty acid	WGDapVKIKKP$_9$GGH$_6$	No palmitoyl	2796 / +4
JB580	Fatty acid	WGDap_aGDap_aVKIKKP$_9$GGH$_6$	2 x Dap-palmitoyl	3416 / +3
JB866	Fatty acid	WGDap_{aa}*VKIKKP$_9$GGH$_6$	2 x palmitoyl	3359 / +3
JB589	Fatty acid	WGC_bVKIKKP$_9$GGH$_6$	Hydrolyzable palmitoyl	3051 / +3
JB858	Fatty acid	WGDab_aVKIKKP$_9$GGH$_6$	Dap →Dab	3046 / +3
JB893	Fatty acid	WGOrn_aVKIKKP$_9$GGH$_6$	Dap → ornithine	3060 / +3
JB894	Fatty acid	WGK_aVKIKKP$_9$GGH$_6$	Dap → lysine	3074 / +3
JB641	Fatty acid	WGDap_cVKIKKP$_9$GGH$_6$	Palmitoyl→ C$_8$ group	2922 / +3
JB621	Fatty acid	W$_c$*$GDap_cVKIKKP_9GGH_6$*	Palmitoyl → 2 xC$_8$ group	3048 / +3
JB729	Fatty acid	WGDap_dVKIKKP$_9$GGH$_6$	Palmitoyl → C$_8$F$_{17}$	3270 / +3
SI-09160	Fatty acid	WGDap_eVKIKKP$_9$GGH$_6$	Palmitoyl → cholesterol	3400 / +3
JB876	Fatty acid	WGC_e*VKIKKP$_9$GGH$_6$	Palmitoyl → cholesterol on Cys	3240 /+3
JB872	Fatty acid	WGC_fVKIKKP$_9$GGH$_6$	Palmitoyl → farnesyl	3017 / +3
JB859	Order	H$_6$GGP$_9$WGDap_aVKIKK	Reversed sequence 1	3034 / +3
JB860	Order	H$_6$GGP$_9$VKIKKDap_aGW	Reversed sequence 2	3034 / +3
JB862	Order	VKIKKWGDap_aP$_9$GGH$_6$	Reordered sequence 3	3034 / +3
JB829-JB26	Control	WGDap_aVKIKKP$_9$G$_4$K-HYNIC-4FB-GLAibA$_2$G$_2$H$_6$	JB577 analog (chemoligation)	4054 / +3
JB434	Control	R$_9$GGLAAAibSGWKH$_6$	Arg$_9$-cell penetrating peptide (CPP)	3200 / +10.5
JB728	Control	WGDap_aVKIKKP$_9$GGK$_g$	Rhodamine-labeled JB577	3025 / +4
JB722	Control	$_g$*$KWGSAibAAALGGR_{10}$*	No His$_6$ / rhodamine-labeled CPP	3249 / +11
JB588	Control	WGDap_aVRRRIRRP$_9$GGK	No His$_6$ / Lys for EDC coupling	2736 / +5
JB586	Control	WGRRVRRRIRRP$_9$GGK	No His$_6$ or palmitoyl / Lys for EDC	2724 / +7.8
JB719	Control	KETWWETWWTEWSQPK$_3$RKVSGAAi-bA$_3$GGH$_6$	Chariot peptide	4297 / +4
JB867	Control	K$_h$GDap_aVKIKKP$_9$GGH$_6$	JB577 with TAMRA dye label	3390 / +4
JB780	Control	$_i$CSTRIDEANQRATKLP$_7$SH$_6$	AF594 FRET acceptor dye on Cys	4182 / +1.5

[a] Prominent peptides are shown shaded. a, palmitoyl (non hydrolyzable); aa*, two palmitoyl attached to same Dap; b, palmitoyl attached to Cys (hydrolyzable); c, C8 octanoyl attached to Dap; c*, C8 octanoyl attached to Trp; d, heptadecafluoroundecanoic acid (C8F17); e, cholesterol; e*, cholesterol attached to Cys; f, farnesyl; g, lissamine rhodamine B attached to Lys or, g*, to N-terminal amine; h, TAMRA attached to Lys; i, Alexa Fluor 594 attached to Cys-thiol. Aib = α-amino isobutyric acid; Dab = diaminobutyric acid; Dap = diaminopropionic acid; Orn = ornithine; HYNIC, hydrazinonicotinoyl; 4FB, 4-formylbenzoyl. Note, we utilize JB577 and JB829-JB26 as functionally interchangeable; the latter is a slightly longer JB577 analog assembled from chemoselective ligation of two-smaller peptides. Relevant structures provided in Supporting Information. All peptides N-terminal acetylated/C-terminal amidated except JB719, JB722. JB = Juan Blanco-Canosa.

TABLE 2. Cellular Uptake, Endosomal Escape, and Viability Results for Selected Peptides

Peptide	Focus	Description	# of COS-1 cells (n)	% QD uptake (n)	% Endosomal escape of total cells (n)	% Escape in cells with uptake	Overall uptake/escape	Cellular viability (%)[a]
JB747	Pro_n-linker	$Pro_9 \rightarrow Aib_9$	78	100% (78)	58% (78)	58%	high/moderate	98 ± 1%
JB865	Pro_n-linker	$Pro_9 \rightarrow Pro_{12}$	82	80% (66)	85% (56)	68%	high/moderate	81 ± 12%
JB864	Pro_n-linker	$Pro_9 \rightarrow Pro_{15}$	99	82% (81)	70% (69)	85%	high/high	92 ± 17%
JB869	Charge	$VKIKKP_5 \rightarrow$ amphipathic-$[VRLP_3]_3$	315	80% (253)	44% (139)	55%	high /moderate	90 ± 9%
JB641	Fatty acid	Palmitoyl → C_8 group	165	50% (83)	44% (73)	88%	moderate/high	105 ± 13%
JB729	Fatty acid	Palmitoyl→ C_8F_{17}	80	64% (51)	54% (43)	84%	high/high	93 ± 12%
SI-09160	Fatty acid	Palmitoyl → cholesterol	102	44% (45)	42% (43)	96%	moderate/high	101 ± 3%
JB858	Fatty acid	Dap →Dab	----	----	>90% membrane localized	----	----	103 ± 3%
JB872	Fatty acid	Palmitoyl → farnesyl	101	99% (100)	78% (79)	79%	high/high	76 ± 7%
JB860	Order	Reversed sequence 2	164	30% (50)	18% (30)	60%	moderate/moderate	58 ± 5%
JB829-JB26	Control	JB577 analog (chemoligation)	60	74% (44)	71% (31)	70%	high/high	101 ± 5%
JB434	Control	Arg_9 cell penetrating peptide	573	82% (469)	0 (0)	0 %	high / none	106 ± 8%
JB728	Control	Rhodamine-labeled JB577	84	81% (68)	76% (63)	93%	high/high	77 ± 7%
JB588[b]	Control	No His_6/ Lys for EDC coupling	64	94% (60)	80% (51)	85%	high/high	ND
JB719	Control	Chariot peptide	180	53% (96)	6% (11)	11%	moderate / low	98 ± 4%
	Cell line	Cell type	# of cells (n)					
JB577	COS-1	African Green Monkey kidney	76	92% (70)	69% (52)	77%	high/high	98 ± 4%
JB577	Hela	human cervical carcinoma	163	90% (147)	77% (126)	86%	high/high	98 ± 1%
JB577	HEK 293	human embryonic kidney	130	69% (89)	59% (77)	86%	high/high	87 ± 5%
JB577	A549	human adenocarcinomic alveolar basal epithelial	69	87% (61)	81% (56)	92%	high/high	96 ± 3%
JB577	PC12	rat adrenal pheochromocytoma	61	75% (46)	68% (42)	91%	high/high	97 ± 10%
JB577	Fibroblasts	Primary human dermal fibroblasts	123	90% (111)	29% (36)	32%	high/moderate	92 ± 6%

[a] Cell viability tested with exposure to 100 nM of 75 peptide/QD. - - - -, not determined. [b] Tested with eBiosciences nanocrystals. A full listing of all results can be found in the Supporting Information.

TAT-peptide.[11] We incubated 100 nM QD-peptide conjugates (~75 peptide/QD valence to ensure saturated loading; slight excess did not affect results, see below) with COS-1 (monkey kidney derived fibroblast-like) cell monolayers for 1−2 h followed by washing and culturing for 48 h prior to fixation and microscopic examination (full procedural description in Materials and Methods and in Supporting Information). Figure 1A shows representative cells exposed to 550 nm QDs assembled with JB577 as well as JB434, an Arg_9-terminated TAT-CPP.[11] JB577-conjugates again appeared well-dispersed throughout the cytosol, occupying the entire cell volume except for nuclei as evidenced by nuclear costaining with DAPI. Endosomal counterstaining with Cy5-labeled transferrin (Tf-Cy5) confirmed the QDs are distinctly separated from these vesicular compartments at 48 h post delivery.[29,30] Notably, endosomal signal remained uniformly punctate - indicative of an intact, undisrupted endocytic pathway. Approximately 90% of cells analyzed showed QD uptake and, of these, ~77% had visible endosomal release with minimal loss of cellular viability (see Table 2 and quantitative delivery discussion below). Confocal micrographs collected through the cell volume itself confirmed the almost uniform, cytosolic distribution of the QDs (Supporting Information Figure S12). Imaging live cells prior to fixation confirmed these observations were not an artifact of fixation (data not shown).[31] Although QD photoluminescence (PL) appears uniformly diffuse in these cells, in certain other cases, diffuse cytosolic QD PL was interdispersed with brighter, punctate PL which we attribute to some QD-peptide material remaining vesicular. In contrast, control cells exposed side-by-side to QD-JB434 showed a tight-punctate, vesicular distribution of QDs which consistently colocalized with the Tf-Cy5 endosomal marker (Figure 1A). This latter result mirrors our previous experience with TAT-peptide delivery of QDs and indeed reflects much of what has been reported for similar constructs in a wide range of cells.[2,6,10,11]

Growth Time and Peptide Valency. Moving beyond confirmation of previous findings, QD-JB577 release to the cytosol over time was next examined (Figure 1B). QD-conjugates were incubated with COS-1 cells as above and imaged at selected time points. Imaging 1 h post-delivery showed QDs adopting a punctate, slightly perinuclear staining that distinctly co-localized with Tf-Cy5 staining (data not shown). At 24 h, QD staining was less perinuclear and appeared to begin accessing the cytosol. By 48 h, a maximal diffuse QD morphology was noted. No appreciable increase in endosomal escape was observed at longer culture time points. To evaluate valency (*i.e.*, peptide ratio: QD) requirements, QDs were assembled with increasing ratios of JB577, delivered to A549 adenocarcinomic human alveolar basal epithelial cells and imaged at 48 h. Representative images in Figure 1C clearly demonstrate that endosomal escape tightly tracks QD-peptide ratio, with maximal effect observed at 75 peptides/QD (*i.e.* maximal loading). Ratios of 19- and 38-peptides/QD show a mixture of punctate and dispersed QD staining while the highest valency shows QD PL that is almost completely cytosolic. Uptake

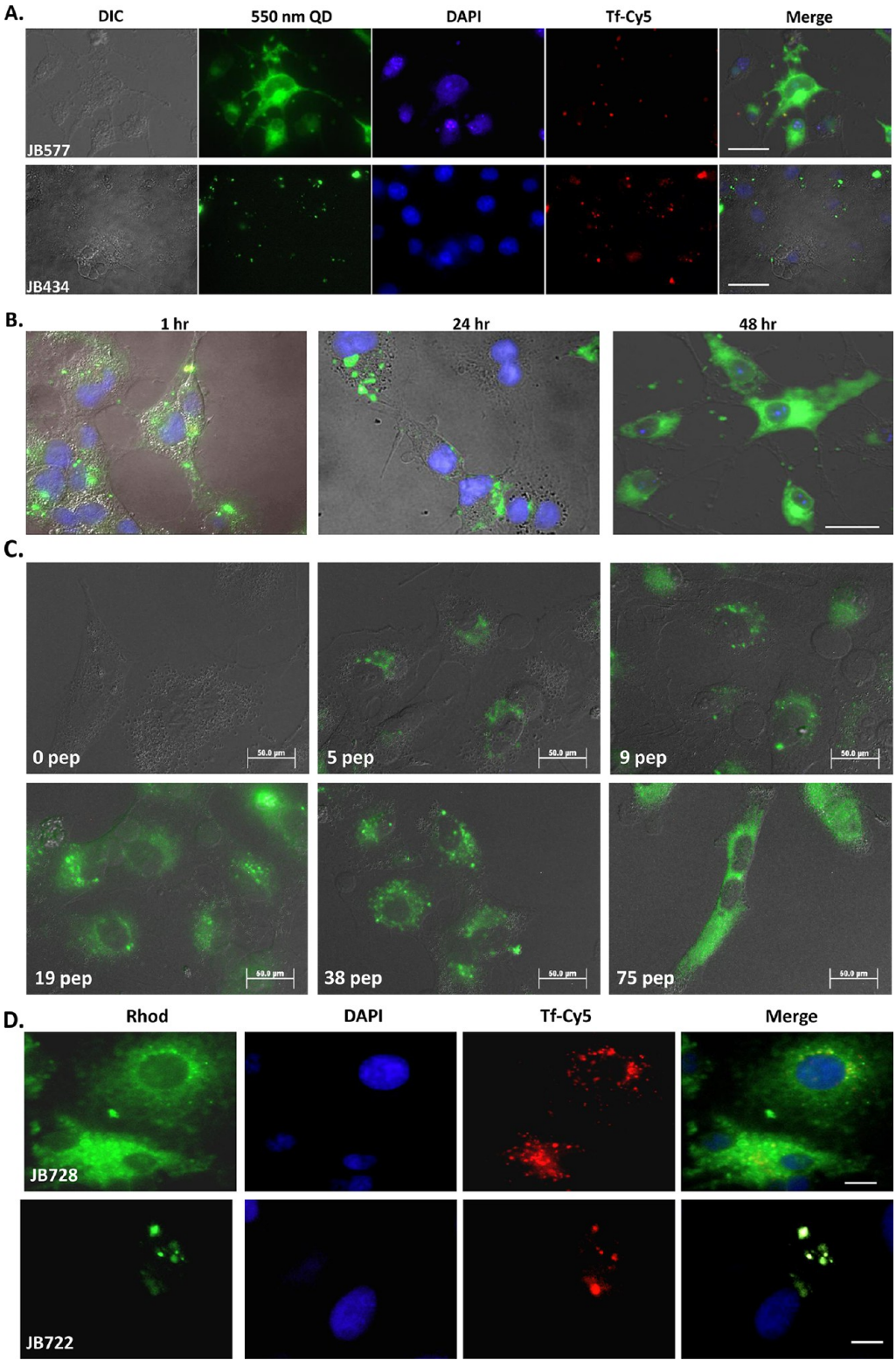

Figure 1. Characterization of JB577-mediated QD delivery. (A) COS-1 cells were co-incubated with 550 nm QDs (100 nM) and 300 nM Cy5-transferrin. QDs were assembled with either 75 JB577 peptides (top) or 30 JB434 peptides/QD (bottom). The latter ratio is used as it is more than adequate for efficient delivery and increasing to 75 does not alter delivery outcome.[11,48] Note PEGylated QDs were utilized throughout unless indicated. (B) COS-1 cells were incubated for 1 h with 550 nm QDs (125 nM) assembled with 75 JB577 peptides/QD. After QD removal and washing, cells were cultured for the times indicated. (C) A549 cells, assembled with the number of JB577 peptides indicated, were incubated for 1 h with 550 nm QDs (100 nM). (D) COS-1 cells labeled with 1 μM rhodamine-labeled JB728 peptide (top) or 1 μM rhodamine-labeled JB722-Arg_{10} cell-penetrating peptide (bottom). False coloring is used here to discriminate between rhodamine and Transferrin-Cy5 fluorescence. For subsequent data, QD-peptides were incubated on cells for 2 h unless otherwise stated. After QD removal and washing, cells were cultured for 48 h prior to fixation and examination. Size bar = 50 μm. Quantum yield of 550 nm QDs ~20% and 625 nm QDs ~60%.

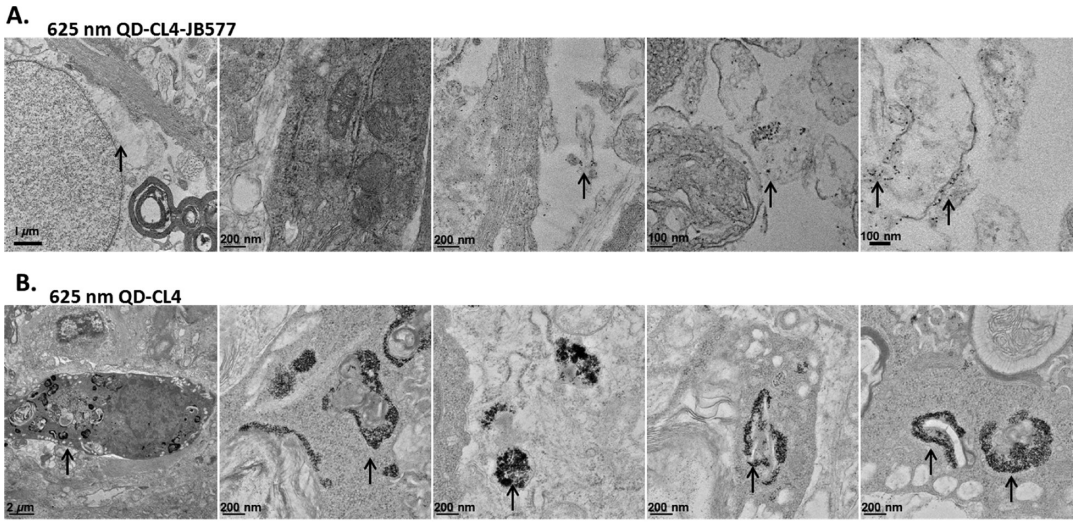

Figure 2. TEM images of QDs in rat hippocampal slice cultures. The 625 nm QDs surface functionalized with CL4 were incubated with rat hippocampal slices in culture for 24 h following which samples were prepared and examined using TEM analysis as described.[32] (A) Representative TEM images for samples exposed to QDs assembled with JB577. The arrows highlight the presence of individual nanocrystals against the cellular background. (B) Representative TEM images for samples exposed to QDs alone. The arrows in this image series highlight the presence of QDs agglomerated and sequestered in what appear to be vesicles or endosomes. An annotated version of this image can be found in the Supporting Information with some of the cellular components of the micrographs identified along with a representative blank control image.

efficiency, as observed from the relative QD PL intensity within each cell, also correlates with peptide valency (*i.e.,* higher peptide:QD ratios resulted in more QD delivery). Given these results, maximal peptide valency and 48 h post-delivery incubation was maintained unless noted.

Peptide Fate and Self-Delivery. To verify that JB577 remained QD-associated and was not proteolytically cleaved or "disassembled" intracellularly, a TAMRA dye-labeled JB577 (JB867) was conjugated onto 625 nm QDs and delivered to COS-1 cells. Fluorescence collected independently from the TAMRA and QD channels had identical staining patterns strongly suggesting the peptide remains QD-associated throughout the uptake/endosomal escape process (Figure S13). These colors/channels were chosen such that QD FRET sensitization of the dye would not take place thus simplifying the analysis. The ability of JB577 to mediate its own endosomal escape was tested in a similar manner with JB728, a sulforhodamine B dye-labeled version, *versus* JB722, a sulforhodamine-labeled TAT-CPP derivative. Figure 1D shows that this JB577 analog undergoes endosomal escape, even in the absence of attachment and display around a central QD platform, yielding a diffuse staining across the cell in contrast to the punctate, endosomal pattern observed for JB722-TAT. However, a similar punctate Tf-Cy5 endosomal staining was noted for both peptide samples.

Transmission Electron Microscopy of QD-JB577 in Fixed Tissue. Given the above results, it was imperative that we collect further corroborating evidence with other experimental means to unequivocally confirm endosomal escape of the QDs. For this we turned to transmission electron microscopy (TEM) and continued working with another more complex tissue model system in which we had previously tested QD-JB577 delivery.[32] As JB577 was originally developed for delivering PPT1 inhibitors specifically to neurons, we had performed studies of QD delivery with this same peptide in *ex vivo* mature rat hippocampal slice cultures. Using 625 nm QDs functionalized with CL4 and conjugated to JB577 we had observed specific delivery of the QDs to neurons. TEM studies in this system are facilitated by the ability to fix, process, slice, and prepare this tissue in a relatively facile manner (as opposed to cellular monolayers grown in culture in a multiwall dish format). Preliminary TEM micrographs of these tissues indicated cytosolic escape of the QD-JB577 conjugates.[32] Continuing on with a more rigorous evaluation of QD escape in this system by TEM analysis, we found that QD-JB577 conjugates (ratio 25/QD) are primarily visualized as individual nanocrystals across the entire cellular cytosol. See for example the representative TEM micrographs in Figure 2A which are shown at different magnifications and where individual QDs appear as small black dots against the cellular background. In stark contrast to this finding, when QD-CL4 samples lacking any peptide were exposed to the same tissue slices in exactly the same manner, the QDs are visualized as dark and dense agglomerations and appear to be specifically sequestered in what appear to be vesicles. In conjunction with the fluorescent imaging results above, this additional data provides very strong experimental evidence supporting the ability of JB577 to facilitate QD escape into the cellular cytosol.

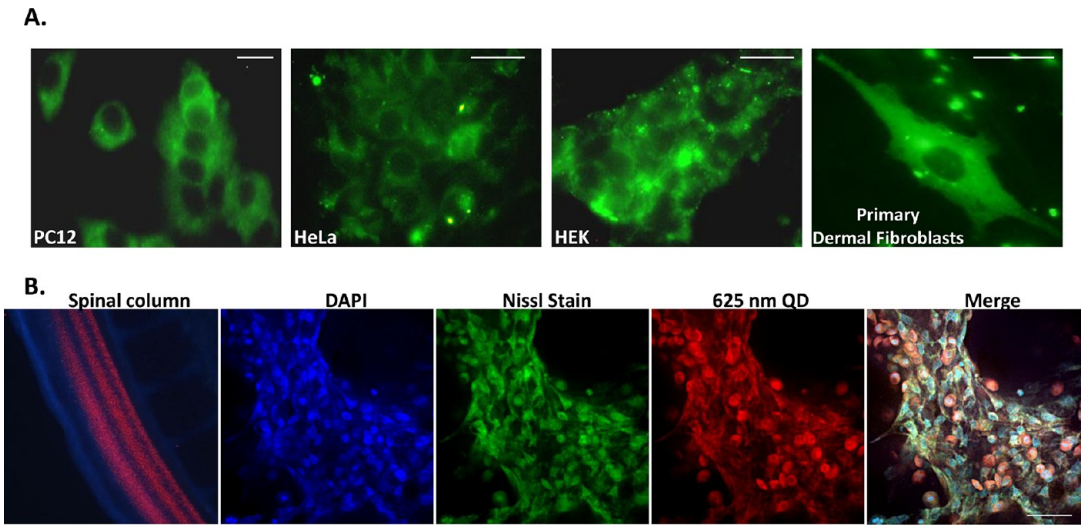

Figure 3. JB577-mediated QD delivery to various cell-lines and tissues. (A) PC12, HeLa, HEK and primary human dermal fibroblast cells were incubated for 2 h with 550 nm QDs (100 nM) assembled with JB577 peptide–QD conjugates as described. Images show cells upon fixation after 48 h in culture. (B) Chick embryos (embryonic day 4) were injected in the lumbar region of the developing spinal column with 625 nm QDs (100 nM) assembled with JB577-QD (25:1) and cultured for 2 more days. Following washing, embryos were fixed and imaged. Left-to-right: image of the developing chick spinal cord showing distribution of injected QDs at day E6 (two days post-injection) and normal morphology, then collapsed (total projection) confocal images highlighting DAPI (nuclei), Nissl (extranuclear RNA), and QD staining along with a merged image. Size bar = 50 μm.

Differing Cell-Lines and Other Tissues. JB577 exhibited similar efficiency in allowing QDs to access the cytosol of other cell-lines representing several tissue-types. As shown in Figure 3A and Table 2, JB577 facilitated robust, comparable cytosolic delivery of QDs in PC12-Adh (adherent rat adrenal pheochromocytoma), HeLa (human cervical carcinoma), HEK (human embryonic kidney 293 cells) and primary human dermal fibroblasts. To test escape in another complex and rapidly growing *in vivo* biological system, JB577-625 nm QD-CL4 conjugates (25:1 ratio) were injected into the spinal cord canal of a developing 4-day old chick embryo (Figure 3B). Following 2 days growth, the embryo was fixed, sectioned into 10 μm thick slices, and imaged with confocal microscopy. QD-conjugates were found distributed throughout the neuroaxis in neuroblasts with significant cytosolic labeling that appeared to be co-localized with Nissl body staining/fluorescence (the latter are extranuclear RNA granules consisting of rough ER and ribosomes). Control experiments where QDs lacking peptide were also injected into the spinal cord of chick embryos did not result in any apparent cytosolic labeling (data not shown). We note that embryonic development continued normally over the 3 days growth with no visible defects or teratogenicity observed. This example, in conjunction with that of the rat hippocampal slice culture above and the same observations in primary fibroblasts, confirms that JB577-mediated endosomal escape of QDs can be robustly applied to both primary and transformed cell lines along with quite complex tissue samples.

Endosomal Escape of Other Nanomaterials. A critical aspect to future JB577 utility would be its ability to mediate endosomal escape of more diverse cargo materials. In contrast to relying on His_6-driven peptide assembly, we began by conjugating commercial 605 nm emitting nanocrystals (NCs, eBioscience) capped with a carboxylated-DSPE-PEG lipid coating (1,2-distearoyl-*sn*-glycero-3-phosphoethanolamine-*N*-[carboxy-(polyethylene glycol)-2000], H_D ~35 nm)[33] to JB588 using standard carbodiimide (EDC) chemistry.[26,33,34] JB588 is a JB577 analog where His_6 and VKIKK were replaced by a unique, terminal lysine (for EDC conjugation to carboxyls) and the VRRRIRR sequence (which displays a similar basic-charge character), respectively. Figure 4A shows images where NC-JB588 conjugates again displayed a cytosolic staining in direct contrast to control NCs coupled to TAT control peptides. We also evaluated protein cargo delivery with maltose binding protein (MBP) displaying a unique D95C residue labeled with Texas Red.[35] This sugar binding protein (MW ~44 kDa; size ~3.0 × 4.0 × 6.5 nm; 51 carboxyl groups with ~84% surface-exposed and available as potential conjugation sites) was similarly EDC-coupled to JB588. COS-1 cells exposed to MBP-JB588 conjugates displayed a well-dispersed cytosolic delivery which was again in stark contrast to cells exposed to MBP-JB586 TAT-controls (Figure 4B). Identical experiments were performed with the far larger *b*-phycoerythrin (*b*-PE) light harvesting complex (MW ~240 kDa, ring structure: 11.0 × 6.0 nm, 222 carboxyl groups with ~67% surface-exposed) and yielded essentially identical results (Figure 4C). Importantly, covalent peptide-modification did not compromise *b*-PE fluorescent properties. As an alternative to proteins, a generation-5 tetramethylrhodamine-labeled poly(amido amine) (PAMAM) dendrimer (MW ~29 kDa, ~5.5 nm diameter)

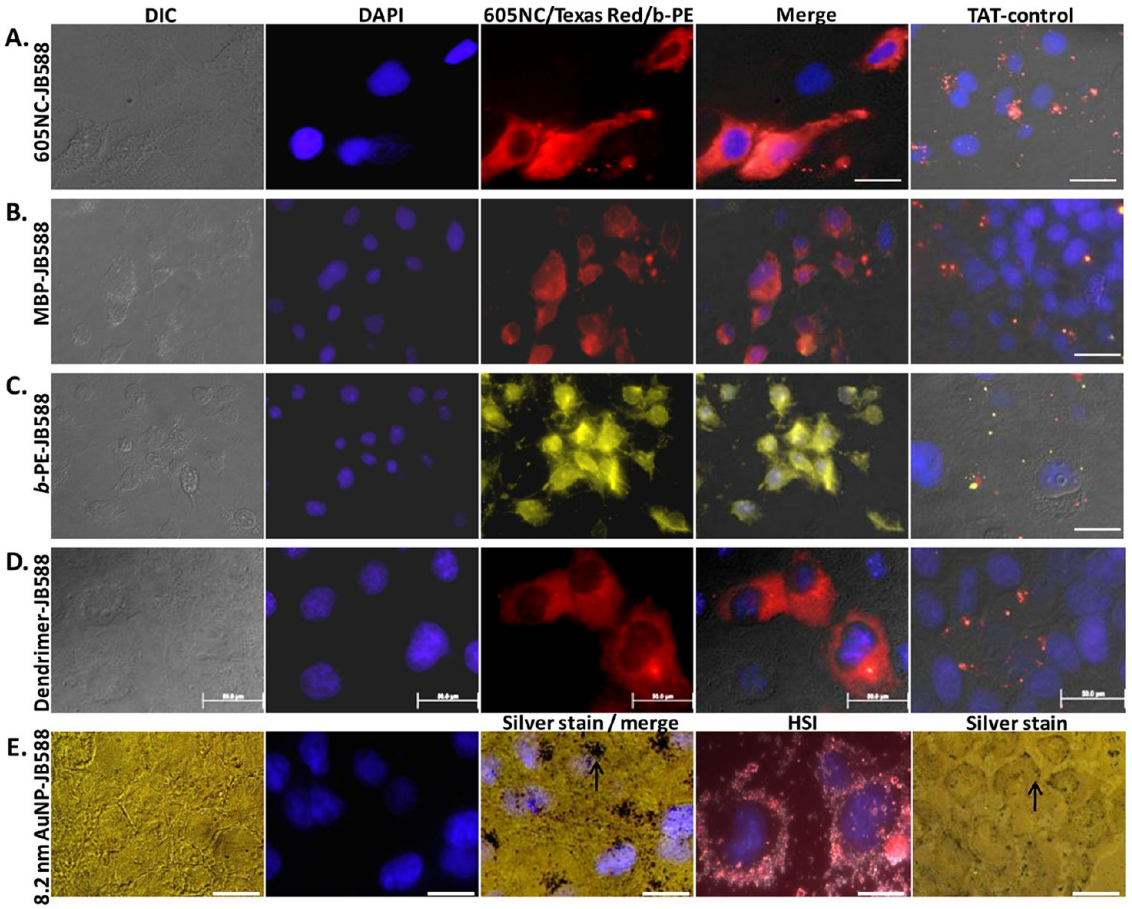

Figure 4. JB577-mediated cytosolic delivery of disparate protein and nanoparticle materials. JB588 peptide EDC-conjugated to (A) eBioscience 605NC (5 nM),[33] (B) Texas Red-labeled maltose binding protein (200 nM), (C) β-phycoerythrin (5 nM),[54] (D) Tetramethylrhodamine isothiocyanate (TRITC)-labeled G5-PAMAM dendrimer (50 nM) and (E) 8.2 nm gold NPs (100 nM, silver stained) and delivered to COS-1 cells as described. All show cytosolic dispersal. Gold NPs localized in what appear to be perinuclear spaces as indicated by the arrow (under Silver stain/merge). See right column of images where a control CPP- (JB586-TAT, Arg_7) conjugate of each species consistently showed NP sequestration within endosomes or alternatively lack of uptake for the gold NPs (arrow under Silver stain indicates AuNPs located at the cell periphery). HSI is hyperspectral imaging which combines simultaneous dark field and fluorescence imaging.[36] In all cases, NP materials were incubated with cells for 1−2 h, washed and cells cultured for 48 h prior to fixation. Magnification: 60× (b and c); 100× (a, d, and e). Size bar = 50 μm except for HSI which is 100 μm.

was covalently coupled to JB588 and provided similar delivery results (Figure 4D). Lastly, we tested 8.2 nm diameter gold nanoparticle- (AuNP) peptide conjugates (Figure 4E). As the AuNPs are not inherently fluorescent, observing their cellular fate was more challenging and we utilized silver staining enhancement and hyperspectral imaging to accomplish this.[36] In this case, AuNP-JB588 manifested a cytosolic/perinuclear delivery pattern (see Figure 4E image under Silver stain/merge) that was proximal to the DAPI nuclear stain. In comparison, the AuNP-TAT-control (JB586) was unable to induce even modest endosomal uptake of the nanoparticle and the materials remained at the cellular membrane or periphery (see Figure 4E image under Silver stain); the latter observation also confirms some of our previous results.[35] Since silver staining prevented observation of Tf-Cy5 fluorescence, it was not possible to confirm cytosolic delivery of the AuNP-JB588 materials. However, it was clear that JB588-conjugation still provided unique uptake attributes including initial cellular uptake which are unavailable to the same size AuNPs functionalized with the control TAT-motif peptide.

Overall, uptake efficiency and endosomal escape of these cargoes was comparable to or even more efficient than for QDs with all cargo distinctly separated from counterstained Tf marker (data not shown). To ensure these deliveries resulted from covalently linked lipopeptide, all constructs were purified by size-exclusion chromatography to remove any remaining "free" peptide. These experiments also show that the putative presence of free peptide in our self-assembled QD constructs above is clearly not an essential requirement for efficient uptake and escape.

Structure Activity Relationship. To provide insight into the role of each motif within JB577 and its contribution toward QD uptake/cytosolic delivery, an iterative SAR analysis was undertaken.[23−25] Modifications to the existing motifs were made and are grouped into four categories in Table 1: (1) Pro_9-linker length, (2) charge,

(3) fatty acid nature along with its attachment chemistry, and (4) presentation order. To comparatively assess among all 29 peptides tested, we implemented a semiquantitative assay which examined individual cells and derived a score for both QD uptake and endosomal escape efficiency. Figure 5A shows representative micrographs from this classification system. For each peptide tested, QD uptake in cells was categorized as: no uptake (no discernible intracellular QD signal), low, moderate or high QD signal. Similarly, the degree of endosomal escape was classified as: membranous (excluded from cell interior), punctate (endosomal), moderate or high endosomal escape. Each peptide was then classified for QD uptake based on cellular scorings as low (<30% cells with uptake), moderate (30−60% uptake), or high (>60% uptake). Endosomal escape was also scored with peptides showing low (<30%), moderate (30−70%) or high (>70%) escape efficiency. Assessments were made from micrographs collected across multiple fields of view in triplicate experiments in direct comparison to results from JB577- (positive control) and JB434- (TAT peptide, negative control) QD conjugates run side-by-side simultaneously. All samples were counterstained with DAPI and Tf-Cy5 to aid in determinations. Table 2 presents results from peptides yielding both moderate to high QD uptake and endosomal escape. Cell numbers examined, quantitative assessment, and cellular viability for each QD-peptide conjugate is also given. See Supporting Table S1 for full results, cellular viability for cells exposed to peptide-alone controls and representative images from other deliveries.

The first motif investigated was Pro_9-linker length (Table 1, Focus: Pro_n-linker). Analogues replaced Pro_9 with: $Pro_{4,12,15}$ (JB582/JB865/JB864); equivalent numbers of the non-natural residue α-isobutyric acid, Aib (JB747) which adopts an α-helical structure;[37] or substitution with either a short Ala_4 or PAA sequence (CS56 Pal-2/CS56 Pal-3). Only JB865/864 displaying the longer $Pro_{12,15}$-repeats or equal numbers of Aib (JB747) maintained a moderate-to-high level of QD uptake and endosomal escape, see Figure 5B for selected results. Charge was next examined (Table 1, Focus: Charge), with peptide variants displaying: 0 (JB578) or 2-VKIKK motifs (JB895), VKIKK replacements with a positively charged/cationic $[VRLPPP]_3$ repeat, and Lys replacement with increased numbers of Arg. The latter two were also tested with (JB583/JB869) and without (JB585/JB868) the palmitoyl group to determine whether that, in conjunction with the charged motif, was capable of mediating all necessary uptake and escape activity. Only JB869 displaying both repeated Arg and palmitoyl yielded significant QD uptake and escape. Similar to JB577, this variant displays nine Pro residues, albeit not contiguously, a similar predicted +3 charge at pH 7.4, along with the presence of Val residues.

Further testing focused on palmitoyl modification and was more complex in nature (see Table 1, Focus: Fatty acid). Of particular interest here was whether this moiety was critical, needed to be presented in a specific position/orientation, contributed generic hydrophobicity/membrane insertion alone, and what influence the lipid-attachment chemistry exerted. The palmitoyl was alternatively replaced with octanoyl (JB641), dioctanoyls (JB621), cholesterol (SI-09160), heptadecafluoroundecanoic acid (C_8F_{17}, JB729) or a farnesyl group (JB872). Cholesterol, C_8F_{17} and farnesyl groups are all known to have strong membrane insertion propensity.[38,39] The Dap used for palmitoyl attachment was also switched to diaminobutyric acid (Dab, JB858), ornithine (orn, JB893), and lysine (JB894) which was intended to extend the side chain length in a stepwise manner by single methylene groups (Figure S2). These modifications allow evaluation of the relationship between the palmitoyl and the peptide backbone along with imparting flexibility to the former for better access/interactions with the membrane. JB876 mimicked the natural reversible *in vivo* palmitoyl attachment by conjugating a hydrolyzable cholesterol to a cysteine-thiol through a unique acetyl linker. Peptide variants displaying one alkane chain (JB641), cholesterol (SI-09160), C_8F_{17} (JB729) or farnesyl (JB872) all demonstrated more efficient endosomal escape than JB577, with the farnesyl also inducing higher initial QD uptake (Figure 5B). Increasing hydrophobicity by doubling the display of palmitoyl (JB580/866) or C_8 (JB621) was counterproductive and lowered cellular uptake.

The nature of palmitoyl/fatty acid attachment proved critical since ester reversibility dramatically lowered uptake (JB589) and completely abrogated escape in the case of cholesterol (JB876), consistent with hydrolysis by endo/lysosomal hydrolases (PPT1 thioesterase or cholesterol esterases). Replacing Dap with orn/lys (JB893/894) also markedly reduced endosomal escape. Replacing Dap with Dab (JB858), increasing the spacing between the peptide backbone and palmitate by *one methylene group* in comparison to JB577, yielded perhaps the most striking result found in this study: QD-JB858 displayed a distinct membranous morphology in PC12-Adh or COS-1 cell monolayers after a 2 h incubation period and distinct labeling of membranous processes extending out from the PC-12 cells can be clearly seen (Figure 5C). Membrane localization was confirmed by confocal images taken through the cells (Figure 5D and Supporting Information). Interestingly, QD-JB858 conjugates remained primarily on the membrane for the 48 h growth time used during initial screening, without affecting cytoviability, indicating a robust association with the extracellular membrane that appeared to preclude internalization. We also examined the N- to C-terminus presentation order of functional modules within JB577 using 3-different rearrangements (JB859/860/862), with only JB860 demonstrating modest activity. Lastly, we tested the Chariot/Pep-1 sequence for QD cellular delivery. This positively

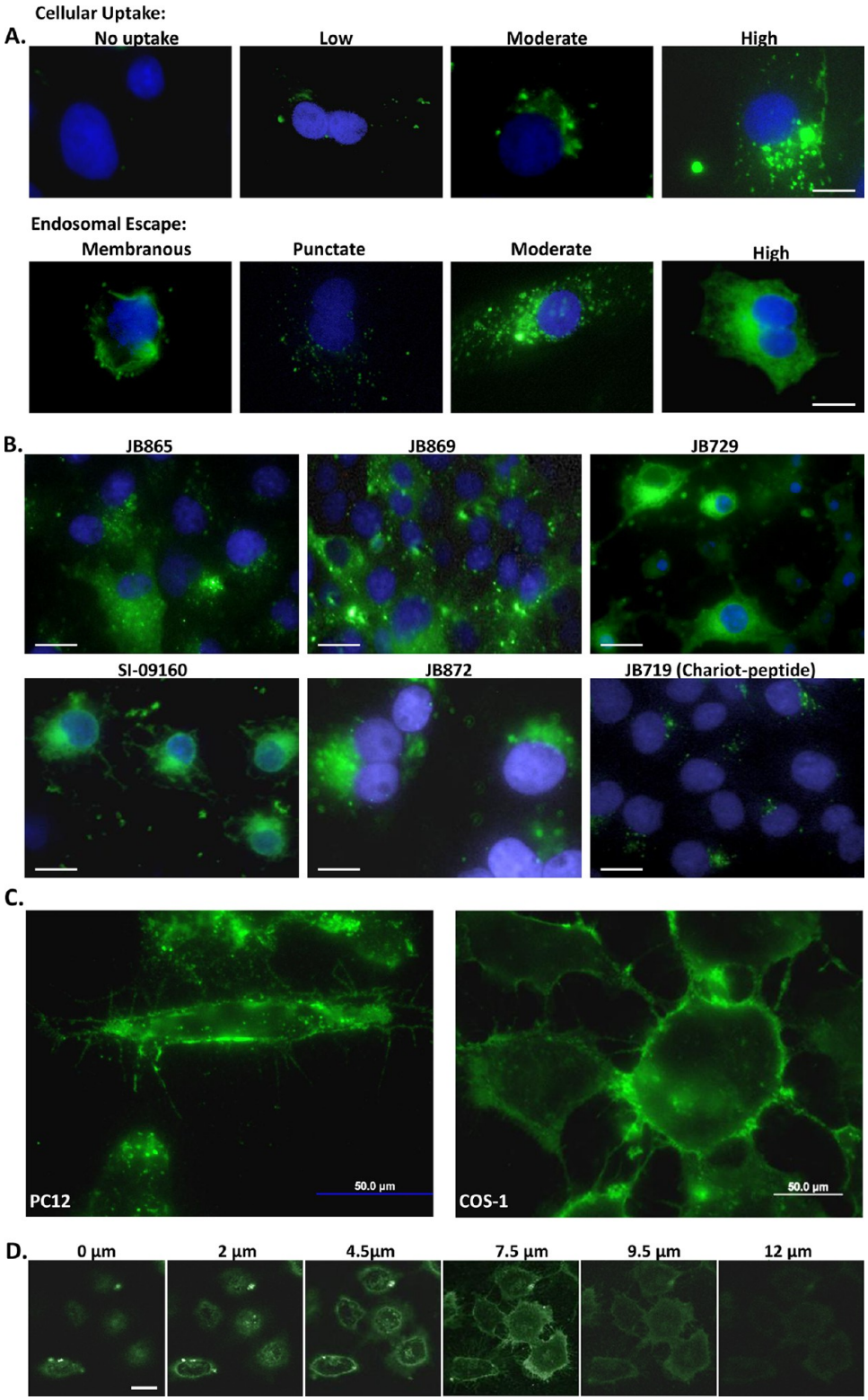

Figure 5. Quantification of QD uptake mediated by JB577 peptide variants. (A) Representative images from the semiquantitative scoring system for uptake of 550 nm QDs (100 nM QD bearing 75 peptides/QD) and endosomal escape in COS-1 cells. Peptide-QDs were incubated with cells for 2 h, removed and cells cultured for 48 h prior to fixation. (B) Peptide variants with uptake/escape activities comparable to JB577 including: JB865 ($Pro_9 \rightarrow Pro_{12}$), JB869 (VKIKKP$_9$ → amphipathic-[VRLP$_3$]$_3$), JB729 (Palmitoyl → C_8F_{17}), SI-09160 (Palmitoyl → cholesterol), JB872 (Palmitoyl → farnesyl). JB719 (Chariot peptide) was used as a comparative control peptide. QDs and delivery conditions are as in (A). (C) JB858 directs QD localization to the plasma membrane. PC12-Adh and COS-1 cells were incubated for 1 h with 550 nm QDs (150 nM) assembled with JB858 peptides/QD followed by washing and fixation. (D) Representative confocal micrographs collected at the indicated sectional height through the COS-1 cells from panel (C). Note the imaging and staining at the 7.5 μm height section corresponding to the cells upper membranes. Size bar = 50 μm.

charged, Trp-rich peptide forms noncovalent complexes with macromolecules - especially proteins - and is believed to rapidly deliver them to the cytosol independent of endocytosis.[21] For QD attachment, the Chariot sequence (JB719) was appended with His_6 and an intervening Ala/Aib helical linker distal to the Trp-rich sequence. QD-JB719 uptake was found to be moderate while endosomal escape was quite low at ~11% (Figure 5B).

DISCUSSION

The single-most important quality initially desired from all the peptide sequences examined here continues from our previous work[11,32] and is that of facilitating endosomal escape. Multiple layers of evidence support peptide-facilitated endosomal escape of QDs (and the other nanomaterials tested here) to the cytosol including: (1) At 48 h post delivery, fluorescence imaging shows the QD-conjugates are localized throughout the cellular cytosol, but not the nucleus, in a solid-uniform staining pattern that extends continuously to the cell periphery, see Figure 1A. (2) The QDs are *not* co-localized with the punctate endosomal transferrin marker at this time point, although both were co-delivered to the cell together and were initially co-localized. (3) Confocal microscopic analysis confirms that the QDs are indeed located within the cytosolic volume and are distinct from the nucleus and endosomes and are further not membrane associated, see Figure S12. For direct comparison, see Figure 5, Figures S10 and S15 which provide confocal confirmation of QD localization to the membrane. (4) Endosomal escape of the same parent QD-peptide conjugate has also now been noted and confirmed in two previous publications.[11,32] (5) Most importantly, TEM analysis confirms that JB577-QD conjugates are located as individual nanocrystals throughout the cellular cytosol even in the cells of complex tissue samples while QDs alone remain sequestered in vesicles in the same experimental format, see Figure 2. Cumulatively, this evidence very strongly suggests the QD−peptide conjugates are indeed cytosolic and indeed we find no evidence to suggest otherwise.

Given the hydrophobic nature of the peptide-appended fatty acids, one important physicochemical issue that concerned us during all the experiments was that of QD−peptide colloidal stability and whether the QD-conjugates aggregated. We thus implemented a functional test of QD-conjugate stability in delivery media prior to cell delivery. This consisted of a 1 min spin at 2000*g* and was repeated during the cell delivery and growth time period at 1, 24, and 48 h. Colloidally unstable QD conjugates aggregate and precipitate under these conditions. We also imaged the cells following delivery to determine if the QD-conjugates had aggregated onto the cell surfaces. See Supporting Information section entitled "Colloidal stability testing of QD-peptide conjugates." These assays revealed that JB833-QD conjugates were not soluble and that JB876 also adversely affected QD stability, see Supporting Information Table S1. In conjunction with this, we also determined the hydrodynamic diameter (H_D) and net charge of the bare QDs and QD-JB577 conjugates in DMEM-HEPES buffer over the 48 h time-period, using dynamic light scattering and zeta potential measurements, respectively, see Supporting Information. Bare QDs appear unperturbed and their H_D does not change significantly during this time-period: 11.5 ± 2.2 nm at 2 h, 12.3 ± 2.3 nm at 24 h, 13.5 ± 2.4 nm at 48 h. We do note an increase in QD-JB577 H_D over the same time frame: 29.3 ± 11.2 nm for 2 h, 43.3 ± 19.0 nm for 24 h, 57.2 ± 17.4 nm for 48 h. The larger initial H_D is expected for this conjugate due to the hydrophobicity and complex solvation properties of the peptide in the context of display around a colloidal nanoparticle. However, in agreement with our assays described above, no larger peaks were noted in the DLS profile which would be indicative of aggregate formation or precipitation. For the latter samples, we attribute the observed increases in H_D over time to QD-peptide conjugate interactions with the many different constituents present in the buffer. Zeta potential measurements (mV) of the bare QDs showed them to be slightly basic in water, *ca.* −15, which dropped to *ca.* −4 to −5 in the buffer. The QD-JB577 conjugate, was slightly positively charged (+8) as expected in water and close to neutral in buffer. These values did not change much with time and again the differences observed between water and buffer are attributed to screening from the many different constituents present in the latter. Overall, we anticipate that similarly complex interactions will take place with the QD−peptide bioconjugates within the intracellular environment, however, this analysis does strongly suggest that aggregates do not form.

These results also shed some light on the overall nature of QD conjugate stability. Prior bioanalytical studies had suggested that a maximum of ~156 to 268 DHLA-PEG ligands (PEG 750 with ~15 ethylene oxide repeats) could be attached to the surface of these QDs depending upon final orientation and packing.[27] Assuming a lower value of ~160 ligands, this means that each QD is essentially held in solution as a colloid by ~2400 ethylene oxide repeats in a somewhat pH independent manner.[26] The parent JB577 peptide is quite hydrophobic and contains 13 hydrophobic residues plus a fatty acid with just 3 hydrophilic-K (cationic) residues. When assembling a saturating level of neutral JB833 (no charged residues) onto the QDs, the resulting JB833-QD conjugates were not soluble in buffer suggesting the charged-KIKK are indeed contributing to the conjugates colloidal stability in many cases. Assuming a loading of ~50 peptides/QD,[27] this translates into ~150 cationic charges which further contribute to QD-conjugate colloidal stability. Without the charged residues present, the hydrophobicity of the peptides (driven by the fatty acids) overcome the PEGs ability to mediate

stability, but addition of a large number of cationic charges can more than compensate for this. Similar to the nature of many other colloidal systems, this suggests that a delicate balance between hydrophobicity and hydrophilicity is required to maintain the fully assembled QD−peptide bioconjugates stable in solution.

Cumulatively, the above results allow us to postulate a preliminary model of essential properties and key steps by which JB577 mediates endosomal escape of QD-conjugates (Figure 6). Early time-point tracking with transferrin co-labeling shows the QD-conjugates and endosome marker consistently together, indicating cellular uptake is probably by endocytosis. However, the exact mechanism (*i.e.*, phagocytosis, pinocytosis, receptor-mediated, clathrin-dependent, *etc.*) is still undefined.[10,29,30] It is also not clear whether polyvalent QD-conjugates and free monovalent peptide are taken up by the same mechanism(s). Conjugate-uptake requires the presence of positively charged Lys/Arg residues, suggesting initial electrostatic interactions with negatively charged cell surface receptors (*i.e.*, heparan sulfate proteoglycans) at the cell membrane in a putative manner that is similar to that believed to occur with the TAT peptide.[40] Lys, however, appears to be preferred over Arg for QD escape as JB583 (Lys → Arg) manifested low uptake and moderate escape. Removing the positively charged residues reduced the percentage of QD uptake almost 10-fold (JB577 92% *vs* JB578 8%).

All experimental peptides that demonstrated moderate-to-high QD escape efficiency also had a predicted charge of +3. Increasing charge beyond +5 (*i.e.*, JB588) decreased both uptake and escape when peptides also displayed a fatty acid. Diminished uptake has been previously noted for TAT-peptides displaying large numbers of Arg.[8] Similarly, the VKIKK sequence by itself and without a fatty acid (JB579) displayed lower uptake efficiency. Taken together, these results suggest synergistic contributions between peptide charge and fatty acid that simultaneously necessitate a functional balancing of charge *vs* lipophilicity. Once membrane-associated, QD-peptide conjugates undergo constitutive endocytosis and are delivered to the cytosol in endocytic vesicles as indicated by Tf-Cy5 counterstaining. Halting endocytosis by incubating cells with QD conjugates at 4 °C did not result in any cellular uptake (data not shown). The process whereby QD-JB577 is taken up by cells and delivered to the endsosomes is identical as to what QD-TAT (JB434) peptide conjugates displayed up to this point and it is also where observed results and putative mechanisms diverge, as we have previously shown that QD-TAT conjugates remain sequestered in the endolysosomal system for >3 days following uptake.[11]

The role of palmitoylation in protein trafficking is complex and beyond the current scope.[15,16,41] That palmitoylation controls membrane association of proteins and is the only dynamic/reversible post-translational fatty acid modification has relevance to the current escape process.[17] Given the native role of palmitoylation in membrane localization, it is probable that some of the palmitoyls appended around the QDs bind the inner membrane when sequestered into endosomes, which may be further driven by local concentration or avidity effects. Simulating JB577 orientation on the QD (Figure 6A) suggests the palmitoyl is displayed extending far beyond the solubilizing PEG coating, resulting in a QD conjugate structure concentrically surrounded by a "corona" or "halo" of positive charge and aliphatic moieties. Supporting avidity effects, examination of JB577 valency (Figure 1C) revealed that maximal peptide valency yielded the most effective QD escape. The ratio of peptide per QD appears to be a more dominant factor than just increasing the concentration of modified particles exposed to cells. For example, eBioscience

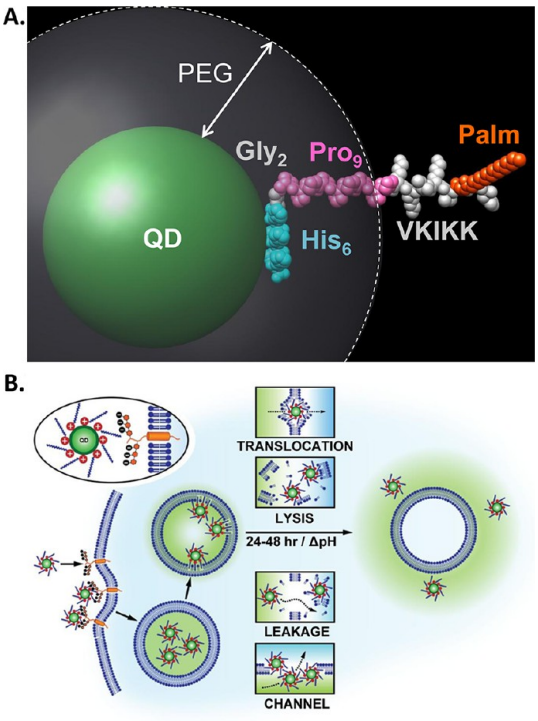

Figure 6. Model of JB577-mediated cytosolic escape of QDs. (A) Simulation of JB577 structure on 550 nm emitting QDs. The 550 nm QD core/shell diameter (~56 Å) and the extension of the PEG ligand on the QD surface (~30 Å) were derived in refs 26, 43. The His_6 sequence (light blue) is assumed to be in contact with the QD surface and does not contribute to lateral extension. This is followed by the Gly_2 flexible linker (gray) and the Pro_9 motif (pink) forms a rigid type II helix. The QD-assembled conformation and extension of the $His_6Gly_2Pro_9$ portion has been previously confirmed with FRET.[44,45,49] The VKIKK sequence is then depicted in gray outside the PEG layer along with the palmitoyl (orange) suggesting that both are available for interactions with the cell membrane. See also Supporting Information. (B) Scheme depicting putative steps in the endocytic uptake of QD-JB577 conjugates. Initial interactions are mediated by the positively charged Lys residues and negatively charged heparan proteoglycan sulfates. Following endosomal formation, the palmitoyls surrounding the QDs penetrate the vesicular membrane. During the next 24−48 h, the QD-peptido-conjugates escape the endosomes in a relatively nontoxic manner and some potential mechanisms are suggested.

NC-conjugate delivery concentration (5 nM) was ~20× lower than the standard 100 nM; this is likely a result of increased carboxylate density available from the lipid micelle coating which would, in turn, allows for an increased ratio of peptide displayed on the QD.

As opposed to endosomal escape of non-QD-conjugated peptide (JB728, Figure 1D), polyvalency is required for cytosolic escape when attached to larger nanoparticle cargoes. This behavior is consistent with the current understanding of single palmitoyl interactions with membranes.[17,41] A single moiety "jitters" on and off the membrane, while a second tethering point significantly stabilizes association and decreases off-rates by several hours. This may contribute to the long residence time in vesicles and the 24-48 h requirement for maximal cytosolic escape. Increasing the peptides aliphatic content by increasing the lipid number displayed (*e.g.*, JB895 2× palmitoyl, JB621 2× octanoyl) decreased escape in all cases. Similar to what was noted for peptide charge *vs* escape efficiency above, increased hydrophobicity appears to be counterproductive suggesting perturbation of a delicate balance in peptide structure−function. Palmitoyl groups are not exclusively required for endosomal escape as functional analogs displaying hydrophobic groups with strong membrane insertion propensity such as octanoyl (JB641), fluorocarbon (JB729), cholesterol (SI-09160), and farnesyl (JB872) groups all demonstrated high escape efficiencies. A nonhydrolyzable linkage between the fatty acid and the peptide is, however, critical as JB589 which contains a palmitoyl attached *via* thioester displayed poor uptake-escape properties. These are presumably susceptible to hydrolysis or esterases resident in the endolysosomal system which remove the fatty acid before some critical step(s). Overall, these studies suggest that the hydrophobic domain must remain intimately associated with the peptide backbone, mimicking the natural post-translational modification of palmitoylated K-Ras.

How the QD-conjugates traverse the vesicular membrane and escape to the cytosol remains unknown although several mechanisms are possible (Figure 6B). It is unclear if the multiple palmitoyl groups displayed around each QD mediate membrane translocation or reorientation, if they form channel-like structures in the membrane that allow QDs to exit, if they completely disrupt the endosomes they are within or, alternatively, allow them to become selectively "leaky." This process, however, requires time (24−48 h) and is minimally cytotoxic, indicating endosomes are not compromised, and the peptide remains attached to the QD throughout. The time factor suggests that concurrent acidification expected within the endosomes may be necessary for efficient escape.[29,30] Indeed, this aspect was incorporated into Brinker's recently designed nanoparticle-supported lipid bilayers which targeted delivery of multiple cargoes to cancer cells.[42] There, acidification protonated a fusogenic peptide sequence displaying His residues and contributed to release by initiating osmotic swelling and destabilizing endosomal membranes *via* a "proton-sponge" mechanism. Such pH-dependent His-effects have not been seen with our peptides over time, almost all of which remain tightly attached to the QDs by Zn(II) coordination of the His_6 even within acidifying endosomes.[11] Torchilin also relied on similar pH changes to enhance targeted intracellular delivery of liposomal preparations.[43]

The Pro_9 helix appears to provide critical rigidity/spacing as designed. It was originally inserted as a rigid linker that would present the (Dap^{Pal})VKIKK segment away from the QD surface extending out beyond the surrounding PEG layer, the latter of which may itself contribute to keeping the peptide from wrapping around the QD surface.[44,45] This presentation would allow cell membranes and their resident receptors to interact with both the charged residues and the palmitoyl (Figure 6). Supporting this, only peptides displaying an equivalent (JB747-Aib_9) or greater number of rigid-spacer residues yielded any significant escape with JB864 (Pro_{15}) even providing for better efficiency. The structural simulation along with the JB747-Aib_9 results suggest the Pro_9 contributes minimal to no CPP-like properties in this context.[20]

The simulation in conjunction with a cumulative examination of the above results again suggests that a delicate balance has to be maintained in the QD-conjugate between Palm presence and the number of charged residues on the peptide along with their location in the overall hybrid structure. This balance functions to provide both colloidal stability and endosomal escape. Consider that the QD-TAT (JB434) construct displays 9-charged Arg residues but does not achieve endosomal escape. Indeed as pointed out in the introduction, almost all TAT functionalized cellular deliveries remain endosomally sequestered. QD-JB833 (neutral) is not colloidally stable while QD-JB895 (2 × VKIKK, displays twice the number of charged residues as JB577) also does not allow for efficient endosomal escape. Only QD-JB577 and structurally similar analogs with minimized charge and fatty acid presence provide for efficient QD endosomal escape. This suggests that, beyond the initial interaction at the cell membrane, the charged moieties on the QD conjugate interact with some target(s) in the endosomes, but this interaction cannot be too strong and the conjugate also requires a fatty acid for ultimate escape from the endosome to the cytosol. In conjunction with this, the order of motif presentation appears important, but not critical, as some peptide sequence rearrangements (JB860, JB869), replacements of Lys with Arg (JB588), and use of peptide analogs assembled by stepwise chemoselective ligation (JB829-JB26) appear to work with the same level of efficiency. As long as key components or overall physicochemical characteristics

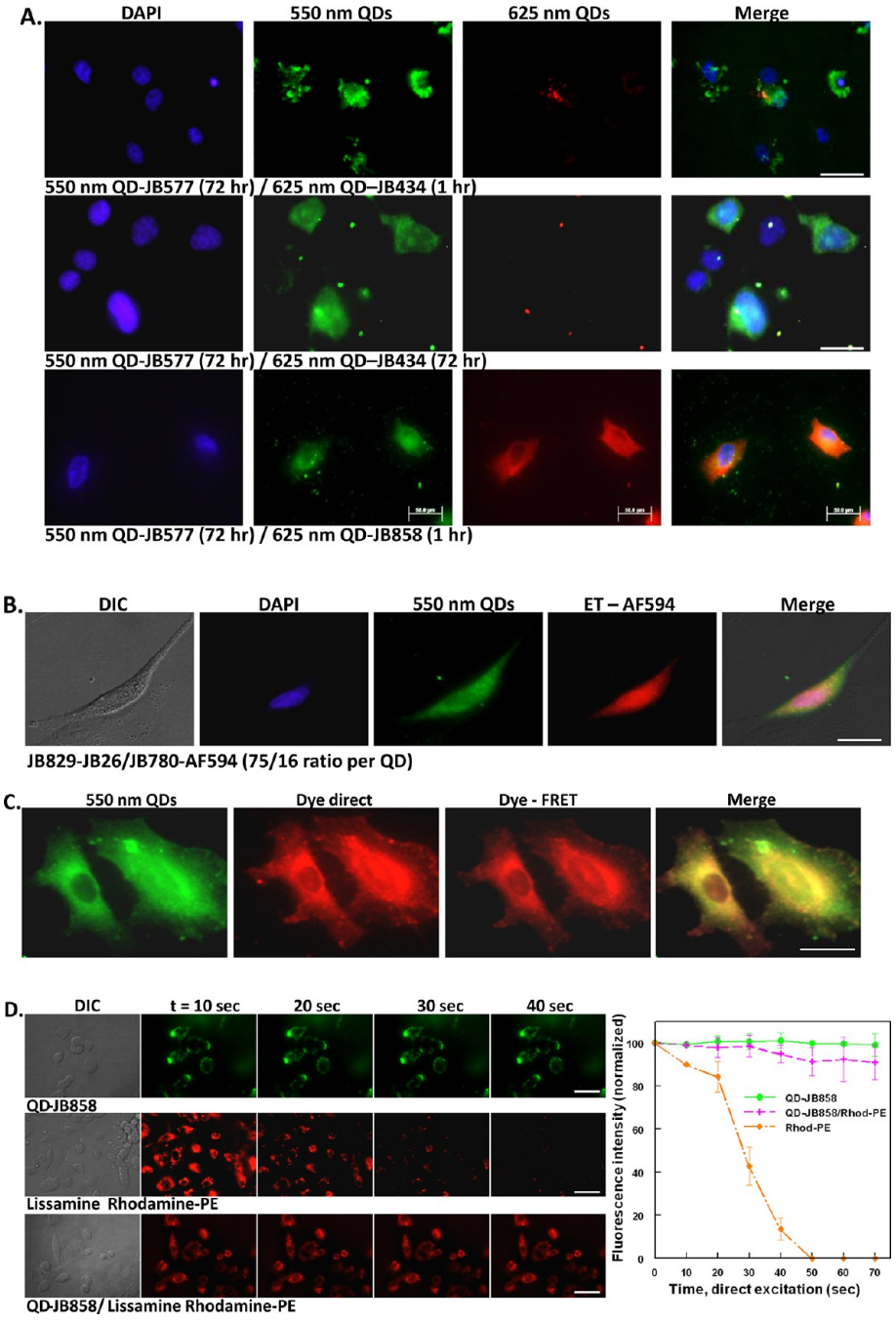

Figure 7. Combinatorial QD–peptide cellular labeling and improved membrane visualization by sensitization. (A) Combinatorial labeling. COS-1 cells labeled with 100 nM 550 nm QDs (75-JB577 peptides/QD; cytosol) and 2 nM 625 nm QDs (20 JB434 peptides/QD; endosomes) by either sequential (top row) or simultaneous incubation (middle row) of the QD-peptide conjugates. Sequential delivery consisted of initial 2 h incubation with QD-JB577 complexes, 72 h cell culture followed by 1 h incubation with QD-JB434 assemblies. For simultaneous incubation, both QD–peptide complexes were incubated on cells for 2 h, removed and cells cultured for 72 h followed by fixation and DAPI-staining. (Bottom row) Sequential labeling of cytosol and plasma membrane of A549 cells with 150 nM 550 nm QDs (75 JB577 peptides/QD, cytosol) and 10 nM 625 nm QDs (75 JB858 peptides/QD, membrane). QD-JB577 assemblies were incubated for 3 h, removed and cells cultured 72 h followed by 1 h incubation with QD-JB858 conjugates prior to fixation. Lower 625 nm QD concentrations are used due to the 3-fold higher Q.Y. (B) Cytosolic QD–peptide cargo delivery and stability. A549 cells were labeled with 550 nm QDs (100 nM) assembled with peptides JB829–26 (75/QD) and AlexaFluor (AF) 594-labeled JB780 (16/QD). QD–peptides were incubated on cells for 3 h followed by 72 h culture period prior to fixation. AF594 is FRET sensitized from direct excitation of the 550 nm QD donor (Förster distance/R_0 ~3.7 nm). (C) Plasma membrane of PC12-Adh cells were labeled sequentially with 125 nM 550 nm QD-JB858 conjugates (1 h incubation) followed by 20 min incubation with 10 μM Rhod-PE. The dye-FRET panel shows sensitization of the dye by the QD donor (R_0 ~5.2 nm). (D) Comparison of the photostability of membrane resident QDs, Lissamine Rhodamine B phosphoethanolamine, and the QD-Rhodamine bilabeled cells. Sensitization circumvents direct dye photobleaching. Full experimental details are given in the Supporting Information. Size bar = 50 μm.

are maintained, similar activity can be provided without adherence to a precise order or strict proximity between motifs. The unexpectedly robust JB858 plasma membrane-targeting highlights the complexity of this peptide's structure–function relationship. This peptide differs from JB577 by only a *single* methylene group (Dap → Dab, see Figure S2), suggesting that exact presentation of the lipid-peptide portion of the conjugate to the membrane may be especially critical here. That this QD conjugate does not enter the endocytic system and remains membrane associated strongly argues for direct interaction(s) with some component(s) of the membrane.[15,16,41] Membrane localization also appears to be unique to the QD-conjugate as dye-labeled JB858 appears to undergo some endocytosis into cells, see Supporting Information.

To provide more insight into peptide mechanics while highlighting labeling utility, we tested if multiple cargos displaying different peptide variants could be co-delivered to cells in a staggered or combined manner (Figure 7). These studies suggested that endosomal escape is specific to individual nanoparticles based on their unique peptidyl display and does not proceed through global disruption of endocytic compartments. For this, green 550 nm QD-JB577 conjugates were first delivered using a 72 h incubation, followed by 1 h cell exposure of red 625 nm QDs-JB434 (Arg_9) conjugates prior to fixing (Figure 7A, top). In the second, both conjugates were delivered simultaneously for 72 h incubation (Figure 7A, middle). Conjugates were co-localized in endosomes during the first hours when co-incubated (data not shown); however, both regimes yielded 550 nm QDs that were completely dispersed throughout the cytosol while 625 nm QDs remained sequestered within vesicles. That both QD species did not adopt a dispersed, cytosolic morphology supports a mechanism whereby QD-loaded endosomes remain largely intact while their membranes become "leaky" in a localized manner, presumably by insertion of multiple palmitoyls. This allows 550 nm QD-JB577 (present at 5× higher concentration in this experiment due to the 3-fold higher 625 nm QD quantum yield) to reach the cytosol while 625 nm QD-JB434 remained sequestered within the vesicles. Related to the hypothesis of a "leaky" and selective escape, we initially tested whether our short or "acute" cell-delivery protocol (~100 nM conjugate/1–2 h cell exposure) contributes significantly to both escape efficiency by a similar process and the remarkable overall lack of toxicity. This regime presumably labels a small cross-section of endosomes without compromising the entire endolysosomal system. As opposed to selective leakage or escape of QDs into the cytosol, a complete undermining of endocytic integrity coupled with a gross release of hydrolytic enzymes would manifest as a significant decrease in cellular viability due to autophagy. Testing of continuous 48 h exposure of select conjugates to COS-1 cells did not significantly decrease cellular viability (97 ± 6%/87 ± 7% and 97 ± 1%/97 ± 2% for JB577- and JB858-QD conjugates/peptide alone, respectively), supporting the notion that the endosomal system is not compromised.

The above conclusions also led us to evaluate other types of dual-labeling utility. In one embodiment, 550 nm QD-JB577 were used in conjunction with 625 nm QD-JB858 conjugates to simultaneously label both the cytosol and plasma membrane (Figure 7A bottom). To verify that QD-lipopeptide conjugates could facilitate cytosolic delivery of an additional cargo on the same NP, 550 nm QDs bearing both a hydrazone conjugated WGDapPalVKIKK (JB829-JB26) and an AlexaFluor 594-labeled control peptide (JB780) were delivered to A549 cells (Figure 7B). Analysis by FRET microscopy again confirmed that these QD-peptide assemblies remained intact within the cytosol over the 3 day culture period and suggested the possibility of conducting intracellular FRET-based sensing with peptide-delivered QD constructs while circumventing reliance on transfection reagents (toxicity) or microinjection (manual, limiting) for delivery. In a last mixed-labeling demonstration, 550 nm QD-JB858 was localized to the membrane of PC12-Adh cells where they were shown to function as potent sensitizers of proximal membrane dyes, see Figure 7C and the Supporting Information for another example. In this configuration, rapid photobleaching from direct dye excitation was significantly mitigated with almost no donor spectral leakage into the acceptor channel (Figure 7D).

CONCLUSIONS

Although elegant physical methods for delivering QDs to the cellular cytosol have been recently developed,[46] the ability to deliver itself, small and large proteins, other QD types, AuNPs and dendrimers to the cellular cytosol in a nontoxic manner suggests that JB577, and several of the other functional peptide analogues described here (JB864, JB872), have much to offer for cellular labeling, drug delivery and theranostic applications where efficient uptake and endosomal escape are both required. Our SAR analysis allowed us to define the key elements within the peptide sequences which must be conserved for cytosolic delivery applications with other (nano)materials. To the best of our knowledge, this is one of the first examples of SAR-type analyses carried out in the context of nanoparticle delivery into cells and suggests that this type of approach may have much to offer for designer bionanotechnology. Further combinatorial and intuitive SAR studies may allow for selection of even more efficient peptides or those displaying other unexpected or designer properties. We note a functional similarity between our sequences and some CPP modifications used to get nucleic acids to escape to the cytosol or to enhance endosomal escape/fusogenic properties.[1,7]

Principal among these are selective lipidation, for example, stearylating CPPs helped improve their DNA delivery capabilities.[7] However, the ability to deliver as wide a range of materials to the cellular cytosol in a variety of cell-lines and tissues and in a relatively nontoxic manner as demonstrated here is currently unknown in any *single* peptidyl entity. The unexpected discovery of a distinct lipopeptide (JB858) with the ability to localize nanoparticles to the cellular membrane may be beneficial for multicolor labeling as demonstrated here. These results also suggest that highly modular peptides expressing several motifs, each capable of providing a different desired function at different points during the process of cellular uptake, may be an alternative design strategy for creating next generation nanoparticle−CPP composites. We realize that there is still much to learn about how these peptides function within the cellular environment. Biochemical assays between relevant proteins and select peptide-conjugates along with evaluation using cells deficient in key endocytic/fatty acid-modification steps are currently in planning. This should not, however, preclude application of the key functional peptide components described here to facilitate cellular uptake and, more importantly, nontoxic endosomal escape of diverse cargos at the growing materials−cellular interface.[47]

MATERIALS AND METHODS

Materials. Human transferrin, Nissl stain, phosphate buffered saline (PBS, 137 mM NaCl, 10 mM phosphate, 3 mM KCl, pH 7.4) and paraformaldehyde were purchased from Sigma (St. Louis, MO). Cy5-succinimidyl ester and PD-10 desalting columns were obtained from GE Healthcare (Piscataway, NJ). Tetramethyl-6-carboxyrhodamine (TAMRA) NHS ester, Alexa Fluor 594-maleimide, β-phycoerythrin, and cell culture grade PBS were purchased from Life Technologies (Carlsbad, CA). All other materials were obtained as noted in the text. Lissamine rhodamine B 1,2-dihexadecanoyl-glycero-3-phosphoethanolamine, triethylammonium salt (referred to herein as Rhod-PE) and 4,4-difluoro-5-(2-thienyl)-4-bora-3a, 4a-diaza-*s*-indacene-3-dodecanoic acid (BODIPY 558/568 C12, referred to as BODIPY dodecanoic acid) were products of Invitrogen (Eugene, OR).

QDs and Capping Ligands. CdSe-ZnS core−shell QDs with emission maxima centered at 550 and 625 nm were synthesized and made hydrophilic by exchanging the native trioctylphosphine/trioctylphosphine oxide (TOP/TOPO) or hydrophobic capping shell with polyethylene glycol MW 750 (average MW 750 Da; PEG750)-appended dihydrolipoic acid (DHLA) ligands terminating in methoxy groups as described previously.[26,50,51] In some cases, QDs were capped with the zwitterionic capping ligand, CL4.[26] The absorption and emission spectra of the QDs and the structures of the capping ligands used in this study are shown in Supporting Information Figure S1. The 605 nm emitting nanocrystals (NCs,) capped with a carboxylated DSPE-PEG lipid coating (1,2-distearoyl-*sn*-glycero-3-phosphoethanolamine-*N*-[carboxy-(polyethylene glycol)-2000], H_D~35 nm) were obtained from eBioscience, San Diego, CA.[33]

Conjugation of Peptides to Various Proteins and Nanoparticles. JB588 was conjugated to various NPs (QDs, proteins, gold NPs, dendrimers) to demonstrate the ability of the peptide to mediate the cytosolic delivery of a range of disparate NP materials. Conjugation to maltose binding protein, β-phycoerythrin and carboxy-DSPE-PEG 605 nm emitting nanocrystals from eBioscience was as described using standard carbodiimide chemistry.[26,34,52]

Conjugation to Gold Nanoparticles. Gold nanoparticles (AuNPs, 8.2 nm diameter) were synthesized as described previously.[53] Briefly, a stock solution of tetrachloroauric (III) acid ($HAuCl_4 \cdot 3H_2O$) was incubated with the desired molar concentration of PEG-modified thioctic acid ligands terminating in carboxy functional groups (TA-PEG600-COOH). AuNP size was controlled by varying the amount of the ligands used and AuNP dispersions were characterized using UV−vis spectroscopy, TEM and DLS. The COOH termini on the ligands served as a target site for EDC-mediated conjugation to the JB588 peptide bearing a terminal primary amine. AuNPs were reacted with JB588 peptide at peptide:surface ligand ratios of ~2.5:1 (corresponding to peptide:AuNP ratios of ~400:1). AuNPs and JB588 peptide were reacted in a 1 mL volume of PBS containing 150 mM EDC and 7.5 mM sulfo-NHS. AuNP-peptide conjugates were purified by using a PD-10 desalting column, concentrated using membrane filtration and stored at 4 °C until use.

Cell Culture and QD−Peptide Delivery. *Cell Culture.* Cell lines were purchased from ATCC (Manassas, VA) and cultured at 37 °C in a humidified atmosphere containing 95% air/5% CO_2. HEK 293T/17, COS-1, HeLa and A549 cells were cultured in Dulbecco's Modified Eagle's Medium (DMEM, purchased from ATCC) supplemented with 10% (v/v) heat-inactivated fetal bovine serum (ATCC) and 1% antibiotic/antimycotic (Sigma). PC12-Adh cells (an adherent variant of the parent PC12 cell line) were cultured in F-12K medium supplemented with 2.5% (v/v) heat-inactivated fetal bovine serum, 12.5% (v/v) horse serum (ATCC) and 1% (v/v) antibiotic/antimycotic. Cells were cultured in T25 flasks and a subculture was performed every 3−4 days. All cells were used between passages 3 and 13. Primary dermal fibroblasts were purchased from ZenBio, Inc. (Research Triangle Park, NC) and were cultured in DMEM containing 10% (v/v) heat-inactivated fetal bovine serum and 1% antibiotic/antimycotic.

QD−Peptide Delivery. QD−peptide bioconjugates were generated by first diluting the appropriate amount of peptide into DMEM containing 25 mM HEPES (DMEM-HEPES) QDs were then added to their final concentration (typically 80−150 nM unless otherwise noted). The mixture was incubated at 25 °C for 20−30 min to allow histidine-mediated peptide−QD self-assembly. Deliveries were performed on adherent cells seeded into the wells of Lab-Tek 8-well chambered #1 borosilicate coverglass (Nalge Nunc, Rochester, NY) that were coated with fibronectin (5−10 μg/mL). QD−peptide bioconjugates were incubated on cell monolayers at 37 °C for 1−3 h as indicated. We seeded 5×10^3 cells per well in the experimental dishes; this typically gives ~$1-1.5 \times 10^4$/well after 48 h of growth under normal conditions. In most cases, endosomes were simultaneously counter-labeled by the inclusion of a transferrin−Cy5 (Tf-Cy5) conjugate (50 μg/mL). After this incubation, the cells were washed with DMEM-HEPES, complete cell growth medium was added and the cells were returned to the incubator and cultured for 48 or 72 h as noted in the text. Prior to imaging, the cells were washed with PBS, fixed with 3.7% paraformaldehyde in PBS (20 min) and nuclei were stained with 1 μg/mL DAPI (Sigma) for 10 min, unless noted otherwise in the text. Imaging and analysis was performed as described in the Supporting Information.

Cellular Delivery of Dye-Labeled Cell-Penetrating Peptides. To determine the ability of CPP and the palmitoyl peptides to mediate their own cellular uptake in the absence of QD cargo, 1 μM of lissamine rhodamine B sulfonyl chloride-labeled CPP or Palm (JB722 and JB728, respectively) was delivered to COS-1 cell monolayers for 2 h in DMEM-HEPES buffer. Media was replaced with complete cell media and cells were allowed to proliferate for 48 h and imaged with a TexasRed filter cube. Endosomes were labeled by the inclusion of a Tf-Cy5 conjugate (50 μg/mL), imaged with a Cy5 filer set. Uptake and escape were calculated for QD/peptide conjugate deliveries as described.

Imaging, Image Analysis, and Quantification of QD Uptake and Endosomal Escape. Cells from each QD−peptide delivery were imaged (see Supporting Information for microscopy methods), classified and ranked by their QD uptake and endosomal escape efficiency using

the semiquantitative ranking criteria described above. This tabulation is a mechanism by which delivery efficacy can be compared and semiquantitatively communicated in total. Peptides with >30% of cells with low, moderate or high QD uptake and/or >30% of cells with moderate or high endosomal escape were considered successful and are shaded in Table 1. Peptides with <30% of cells with these designations were considered unsuccessful. Representative images from these peptide deliveries are shown in Supporting Information Figure S5. The endosomal escape of JB577 peptide-delivered QDs was also confirmed by confocal microscopy (z-stack imaging, see Supporting Information). Live cell imaging was also performed to confirm that the intracellular fate of JB577 peptide–QD complexes was not attributable to cellular fixation protocols as has been reported previously for some cell-penetrating peptide-delivered cargos (see Supporting Information).[31]

Colabeling of Plasma Membrane with QD–Peptides and Membrane-Labeling Dyes. The ability of peptide–QD bioconjugates delivered specifically to the plasma membrane to engage in FRET with membrane-labeling fluorophores was assessed in PC12-Adh cells. The plasma membrane was first labeled with QD-peptide conjugates (550 nm QDs appended with JB858 peptides) by incubating cell monolayers with the conjugates for 1 h at 37 °C. The cells were subsequently washed once with PBS and then incubated with either 10 μM Rhod-PE (Invitrogen; ex. 560 nm/em. 580 nm) or 5 μM BODIPY dodecanoic acid (Invitrogen; ex. 558 nm/em. 568 nm) in DMEM-HEPES for 20 min at room temperature. The cells were then washed once with PBS and fixed prior to imaging. Imaging of the QD-sensitized Rhod-PE dye was done using the filter configuration described in Supporting Information Table S3. To demonstrate the photostability of the QDs and how their FRET excitation of Rhod-PE acceptors circumvents dye photobleaching, experiments were conducted wherein the membranes of PC-12-Adh cells were colabeled with both the QDs and Rhod-PE dyes. Over a time course of 70 s of constant UV illumination, we quantified the fluorescence intensity of the QD and dye when each species was excited directly. We also quantified the fluorescence intensity of the dye when excited in a FRET configuration with the QD as donor. Control images for showing no leakage of donor and acceptor into opposite channels are shown in Supporting Information Figure S6b.

Peptide-Mediated Delivery and Imaging of Various Nanoparticle Materials. JB588 peptide (JB577 equivalent bearing a terminal lysine) was covalently conjugated to dye-labeled maltose-binding protein (MBP), β-phycoerythrin (β-PE), dye-labeled G5 PAMAM dendrimer and 8.2 nm colloidal gold NPs (AuNPs). The conjugates were diluted into DMEM containing 25 mM HEPES and incubated with COS-1 cell monolayers at 37 °C for 2 h, removed, and the cells were cultured for 48 h followed by fixation as described previously. Cells labeled with AuNPs were silver stained for ~5 min using a silver staining enhancer kit (Sigma). The MBP, β-PE and dendrimer samples were imaged using a Texas Red filter set. AuNP samples were imaged as described in the Supporting Information.

Delivery of QDs to Developing Chick Embryo and Rat Hippocampal Slices. Fertilized chicken eggs were incubated at 37.9 °C and 60% humidity in a Midwest incubator for three days. Eggs were then placed on their sides for at least 30 min before opening. An aliquot (3 μL) of albumin was removed with a syringe from a small hole at the blunt end of the egg. Chick embryos at embryonic day 4 (E4) were injected in the lumbar region of the developing spinal cord using a glass capillary needle with 3 μL of 625 nm QDs (100 nM) assembled with 25 JB577 peptides. The chicken embryos are made directly accessible by cutting a window in the eggshell and carefully removing the extraembryonic membranes covering the embryo, using forceps and spring scissors. Injection of a mixture of QD and methyl green (10:1) into the central canal of the spinal cord was performed with a glass capillary needle into the portion displayed by windowing. The maximum injection volume (around 3 μL) was achieved when the dye had reached the brain vesicle. After retraction of the capillary, the window in the eggshell was resealed with tape. Embryos were allowed to continue growing and developing for three more days where the QDs are seen along the spinal cord and translocated through to ventricles to the cerebellum and other developing brain structures (see Supporting Information Figure S8). Embryos were then fixed and stained with DAPI (nuclei) and with an aniline stain for Nissl bodies/granules (neurons). The QD distribution was visualized with 40× confocal imaging (see microscopy details in the Supporting Information). QD delivery to rat hippocampal slices was as described.[32] The TEM staining protocol is provided in the Supporting Information. Experiments were all IRB approved and met all institutional animal handling requirements where necessary.

Conflict of Interest: The authors declare no competing financial interest.

Acknowledgment. The authors thank K. Sapsford (FDA) for imaging assistance and acknowledge DARPA, NRL NSI, DTRA JSTO MIPR # B112582M. We thank Invitrogen/Life Technologies for the 625 nm QDs. J.B.B.-C. acknowledges a Marie Curie IOF (220292). S.C.D. acknowledges the Louisiana Cancer Research Consortium and NIH Grant Number 5G12RR026260-03 from the National Center for Research Resources. W.R.A. is grateful to the Natural Sciences and Engineering Research Council of Canada (NSERC) for a postdoctoral fellowship. G.D. acknowledges USPHS HD09402. Molecular graphics images were produced using the UCSF Chimera package from the Resource for Biocomputing, Visualization, and Informatics at the University of California, San Francisco (supported by NIH P41 RR-01081).

Supporting Information Available: Full description of the remaining materials and methods including detailed peptide synthesis, dendrimer synthesis and labeling, all delivery results, cytotoxicity testing, along with details of the microscopy and imaging methods used. Representative images, selected results and discussion are also provided. This material is available free of charge *via* the Internet at http://pubs.acs.org.

REFERENCES AND NOTES

1. El-Sayed, A.; Futaki, S.; Harashima, H. Delivery of Macromolecules Using Arginine-Rich Cell-Penetrating Peptides: Ways to Overcome Endosomal Entrapment. *AAPS J.* **2009**, *11*, 13–22.
2. Fonseca, S. B.; Pereira, M. P.; Kelley, S. O. Recent Advances in the Use of Cell-Penetrating Peptides for Medical and Biological Applications. *Adv. Drug Delivery Rev.* **2009**, *61*, 953–964.
3. Gupta, B.; Levchenko, T. S.; Torchilin, V. P. Intracellular Delivery of Large Molecules and Small Particles by Cell-Penetrating Proteins and Peptides. *Adv. Drug Delivery Rev.* **2005**, *57*, 637–651.
4. Juliano, R. L.; Alam, R.; Dixit, V.; Kang, H. M. Cell-Targeting and Cell-Penetrating Peptides for Delivery of Therapeutic and Imaging Agents. *Wiley Interdiscip. Rev. Nanomed. Nanobiotechnol.* **2009**, *1*, 324–335.
5. Torchilin, V. P. Cell Penetrating Peptide-Modified Pharmaceutical Nanocarriers for Intracellular Drug and Gene Delivery. *Pept. Sci.* **2008**, *90*, 604–610.
6. Delehanty, J. B.; Mattoussi, H.; Medintz, I. L. Delivering Quantum Dots into Cells: Strategies, Progress and Remaining Issues. *Anal. Bioanal. Chem.* **2009**, *393*, 1091–110.
7. Nakase, I.; Akita, H.; Kogure, K.; Gräslund, A.; Langel, U.; Harashima, H.; Futaki, S. Efficient Intracellular Delivery of Nucleic Acid Pharmaceuticals Using Cell-Penetrating Peptides. *Acc. Chem. Res.* **2012**, *45*, 1132–1139.
8. Zhao, M.; Weissleder, R. Intracellular Cargo Delivery Using Tat Peptide and Derivatives. *Med. Res. Rev.* **2004**, *24*, 1–12.
9. Foerg, C.; Merkle, H. P. On the Biomedical Promise of Cell Penetrating Peptides: Limits *versus* Prospects. *J. Pharm. Sci.* **2008**, *97*, 144–162.
10. Iversen, T.-G.; Skotland, T.; Sandvig, K. Endocytosis and Intracellular Transport of Nanoparticles: Present Knowledge and Need for Future Studies. *Nano Today* **2011**, *6*, 176–185.
11. Delehanty, J. B.; Bradburne, C. E.; Boeneman, K.; Susumu, K.; Farrell, D.; Mei, B. C.; Blanco-Canosa, J. B.; Dawson, G.; Dawson, P. E.; Mattoussi, H.; *et al.* Delivering Quantum Dot-Peptide Bioconjugates to the Cellular Cytosol: Escaping from the Endolysosomal System. *Integr. Biol.* **2010**, *2*, 265–277.
12. Bayles, A. R.; Bayles, A. R.; Chahal, H. S.; Chahal, D. S.; Goldbeck, C. P.; Cohen, B. E.; Helms, B. A. Rapid Cytosolic Delivery of Luminescent Nanocrystals in Live Cells with

Endosome-Disrupting Polymer Colloids. *Nano Lett.* **2010**, *10*, 4086–4092.
13. Kobayashi, S.; Nakase, I.; Kawabata, N.; Yu, H. H.; Pujals, S.; Imanishi, M.; Giralt, E.; Futaki, S. Cytosolic Targeting of Macromolecules using a pH-Dependent Fusogenic Peptide in Combination with Cationic Liposomes. *Bioconjugate Chem.* **2009**, *20*, 953–959.
14. Dawson, G.; Schroeder, C.; Dawson, P. E. Palmitoyl:Protein Thioesterase (PPT1) Inhibitors Can Act as Pharmacological Chaperones in Infantile Batten Disease. *Biochem. Biophys. Res. Commun.* **2010**, *395*, 66–69.
15. Aicart-Ramos, C.; Valero, R. A.; Rodriguez-Crespo, I. Protein Palmitoylation and Subcellular Trafficking. *Biochim. Biophys. Acta* **2011**, *1808*, 2981–2994.
16. Linder, M. E.; Deschenes, R. J. Palmitoylation: Policing Protein Stability and Traffic. *Nat. Rev. Mol. Cell. Biol.* **2007**, *8*, 74–84.
17. Rocks, O.; Gerauer, M.; Vartak, N.; Koch, S.; Huang, Z. P.; Pechlivanis, M.; Kuhlmann, J.; Brunsveld, L.; Chandra, A.; Ellinger, B.; *et al.* The Palmitoylation Machinery is a Spatially Organizing System for Peripheral Membrane Proteins. *Cell* **2010**, *141*, 458–471.
18. Sapsford, K. E.; Pons, T.; Medintz, I. L.; Higashiya, S.; Brunel, F. M.; Dawson, P. E.; Mattoussi, H. Kinetics of Metal-Affinity Driven Self-Assembly Between Proteins or Peptides and CdSe-ZnS Quantum Dots. *J. Phys. Chem. C* **2007**, *111*, 11528–11538.
19. Sapsford, K. E.; Farrell, D.; Sun, S.; Rasooly, A.; Mattoussi, H.; Medintz, I. L. Monitoring of Enzymatic Proteolysis on a Electroluminescent-CCD Microchip Platform Using Quantum Dot-Peptide Substrates. *Sens. Actuators, B* **2009**, *139*, 13–21.
20. Pujals, S.; Bastus, N. G.; Pereiro, E.; Lopez-Iglesias, C.; Punte, V. F.; Kogan, M. J.; Giralt, E. Shuttling Gold Nanoparticles into Tumoral Cells with an Amphipathic Proline-Rich Peptide. *ChemBioChem* **2009**, *10*, 1025–1031.
21. Archdeacon, D. Chariot™, A Peptide Carrier for the Delivery of Biologically Active Proteins into Mammalian Cells. *Nat. Methods* **2006**, Appl. Notes. DOI:10.1038/an1706.
22. Zhang, W.; Song, J. J.; Zhang, B. Z.; Liu, L. W.; Wang, K. R; Wang, R. Design of Acid-Activated Cell Penetrating Peptide for Delivery of Active Molecules into Cancer Cells. *Bioconjugate Chem.* **2011**, *22*, 1410–1415.
23. Khandare, J.; Minko, T. Polymer-Drug Conjugates: Progress in Polymeric Prodrugs. *Prog. Polym. Sci.* **2006**, *31*, 359–397.
24. Wawer, M.; Bajorath, J. Extraction of Structure-Activity Relationship Information from High-Throughput Screening Data. *Curr. Med. Chem.* **2009**, *16*, 4049–4057.
25. Erhardt, P. W.; Proudfoot, J. R. Drug Discovery: Historical Perspective, Current Status, and Outlook. *Compr. Med. Chem. II* **2007**, *1*, 29–96.
26. Susumu, K.; Oh, E.; Delehanty, J. B.; Blanco-Canosa, J. B.; Johnson, B. J.; Jain, V.; Hervey, W. J.; Algar, W. R.; Boeneman, K.; Dawson, P. E.; *et al.* Multifunctional Compact Zwitterionic Ligands for Preparing Robust Biocompatible Semiconductor Quantum Dots and Gold Nanoparticles. *J. Am. Chem. Soc.* **2011**, *133*, 9480–9496.
27. Prasuhn, D. E.; Deschamps, J. R.; Susumu, K.; Stewart, M. A.; Boeneman, K.; Blanco-Canosa, J. B.; Dawson, P. E.; Medintz, I. L. Polyvalent Display and Packing of Peptides and Proteins on Semiconductor Quantum Dots: Predicted *versus* Experimental Results. *Small* **2009**, *6*, 555–564.
28. Algar, W. R.; Wegner, D.; Huston, A.; Blanco-Canosa, J.; Stewart, M. H.; Armstrong, A.; Dawson, P. E.; Hildebrandt, N.; Medintz, I. L. Quantum Dots as Simultaneous Acceptors and Donors in Time-Gated Förster Resonance Energy Transfer Relays: Characterization and Biosensing. *J. Am. Chem. Soc.* **2012**, *134*, 1876–1891.
29. Canton, I.; Battaglia, G. Endocytosis at the Nanoscale. *Chem. Soc. Rev.* **2012**, *41*, 2718–2739.
30. Mayle, K. M.; Le, A. M.; Kamei, D. T. The Intracellular Trafficking Pathway of Transferrin. *Biochim. Biophys. Acta* **2012**, *1820*, 264–281.
31. Richard, J. P.; Melikov, K.; Vives, E.; Ramos, C.; Verbeure, B.; Gait, M. J.; Chernomordik, L. V.; Lebleu, B. Cell-Penetrating Peptides. A Reevaluation of the Mechanism of Cellular Uptake. *J. Biol. Chem.* **2003**, *278*, 585–590.
32. Walters, R.; Kraig, R. P.; Medintz, I.; Delehanty, J. B.; Stewart, M. H.; Susumu, K.; Huston, A. L.; Dawson, P. E.; Dawson, G. Nanoparticle Targeting to Neurons in a Rat Hippocampal Slice Culture. *ASN Neuro* **2012**, *4*, No. art:e00099.
33. Jennings, T. L.; Becker-Catania, S. G.; Triulzi, R. C.; Tao, G. L.; Scott, B.; Sapsford, K. E.; Spindel, S.; Oh, E.; Jain, V.; Delehanty, J. B.; *et al.* Reactive Semiconductor Nanocrystals for Chemoselective Biolabeling and Multiplexed Analysis. *ACS Nano* **2011**, *5*, 5579–5593.
34. Hermanson, G. T. *Bioconjugate Techniques*, 2nd ed.; Academic Press: San Diego, CA, 2008.
35. Medintz, I. L.; Goldman, E. R.; Lassman, M. E.; Mauro, J. M. A Fluorescence Resonance Energy Transfer Sensor Based on Maltose Binding Protein. *Bioconjugate Chem.* **2003**, *14*, 909–918.
36. Oh, E.; Delehanty, J. B.; Sapsford, K. E.; Susumu, K.; Goswami, R.; Blanco-Canosa, J. B.; Dawson, P. E.; Granek, J.; Shoff, M.; Zhang, Q.; *et al.* Cellular Uptake and Fate of PEGylated Gold Nanoparticles is Dependent on Both Cell-Penetration Peptides and Particle Size. *ACS Nano* **2011**, *5*, 6434–6448.
37. Banerjee, R.; Basu, G.; Chene, P.; Roy, S. Aib-Based Peptide Backbone as Scaffolds for Helical Peptide Mimics. *J. Pept. Res.* **2002**, *60*, 88–94.
38. Shao, S. C.; Hegde, R. S. Membrane Protein Insertion at the Endoplasmic Reticulum. *Ann. Rev. Cell Dev. Biol.* **2011**, *27*, 25–56.
39. Schleiff, E.; Soll, J. Membrane Protein Insertion: Mixing Eukaryotic and Prokaryotic Concepts. *EMBO Rep.* **2005**, *6*, 1023–1027.
40. Fuchs, S. M.; Raines, R. T. Pathway for Polyarginine Entry into Mammalian Cell. *Biochemistry* **2004**, *43*, 2438–2444.
41. Conibear, E.; Davis, N. G. Palmitoylation and Depalmitoylation Dynamics at a Glance. *J. Cell Sci.* **2010**, *123*, 4007–4010.
42. Ashley, C. E.; Carnes, E. C.; Phillips, G. K.; Padilla, D.; Durfee, P. N.; Brown, P. A.; Hanna, T. N.; Liu, J. W.; Phillips, B.; Carter, M. B.; *et al.* The Targeted Delivery of Multicomponent Cargos to Cancer Cells by Nanoporous Particle-Supported Lipid Bilayers. *Nat. Mater.* **2011**, *10*, 389–397.
43. Sawant, R. M.; Hurley, J. P.; Salmaso, S.; Kale, A.; Tolcheva, E.; Levchenko, T. S.; Torchilin, V. P. "SMART" Drug Delivery Systems: Double-Targeted pH-Responsive Pharmaceutical Nanocarriers. *Bioconjugate Chem.* **2006**, *17*, 943–949.
44. Boeneman, K.; Prasuhn, D. E.; Blanco-Canosa, J. B.; Dawson, P. E.; Melinger, J. S.; Ancona, M.; Stewart, M. H.; Susumu, K.; Huston, A.; Medintz, I. L. Self-Assembled Quantum Dot-Sensitized Multivalent DNA Photonic Wires. *J. Am. Chem. Soc.* **2010**, *132*, 18177–18190.
45. Boeneman, K.; Deschamps, J. R.; Buckhout-White, S.; Prasuhn, D. E.; Blanco-Canosa, J. B.; Dawson, P. E.; Stewart, M. H.; Susumu, K.; Goldman, E. R.; Ancona, M.; *et al.* Quantum Dot DNA Bioconjugates: Attachment Chemistry Strongly Influences the Resulting Composite Architecture. *ACS Nano* **2010**, *4*, 7253–7266.
46. Xu, J.; Teslaa, T.; Wu, T. H.; Chiou, P. Y.; Teitell, M. A.; Weiss, S. Nanoblade Delivery and Incorporation of Quantum Dot Conjugates into Tubulin Networks in Live Cells. *Nano Lett.* **2012**, *12*, 5669–5672.
47. Mager, M. D.; LaPointe, V.; Stevens, M. M. Exploring and Exploiting Chemistry at the Cell Surface. *Nat. Chem.* **2011**, *3*, 582–589.
48. Delehanty, J. B.; Medintz, I. L.; Pons, T.; Brunel, F. M.; Dawson, P. E.; Mattoussi, H. Self-Assembled Quantum Dot-Peptide Bioconjugates for Selective Intracellular Delivery. *Bioconjugate Chem.* **2006**, *17*, 920–927.
49. Blanco-Canosa, J. B.; Medintz, I. L.; Farrell, D.; Mattoussi, H.; Dawson, P. E. Rapid Covalent Ligation of Fluorescent Peptides to Water Solubilized Quantum Dots. *J. Am. Chem. Soc.* **2010**, *132*, 10027–10033.
50. Mei, B. C.; Susumu, K.; Medintz, I. L.; Mattoussi, H. Polyethylene Glycol-Based Bidentate Ligands to Enhance Quantum Dot and Gold Nanoparticle Stability in Biological Media. *Nat. Protoc.* **2009**, *4*, 412–423.

51. Mei, B. C.; Susumu, K.; Medintz, I. L.; Delehanty, J. B.; Mountziaris, T. J.; Mattoussi, H. Modular Poly(ethylene glycol) Ligands for Biocompatible Semiconductor and Gold Nanocrystals with Extended pH and Ionic Stability. *J. Mat. Chem.* **2008**, *18*, 4949–4958.
52. Prasuhn, D. E.; Feltz, A.; Blanco-Canosa, J. B.; Susumu, K.; Stewart, M. H.; Mei, B. C.; Yakovlev, A.; Loukov, C.; Mallet, J. M.; Oheim, M.; *et al.* Quantum Dot Peptide Biosensors for Monitoring Caspase 3 Proteolysis and Calcium Ions. *ACS Nano* **2010**, *4*, 5487–5497.
53. Oh, E.; Susumu, K.; Goswami, K.; Mattoussi, R.; One-Phase, H. Synthesis of Water-Soluble Gold Nanoparticles with Control over Size and Surface Functionalities. *Langmuir* **2010**, *26*, 7604–7613.
54. Medintz, I. L.; Pons, T.; Susumu, K.; Boeneman, K.; Dennis, A.; Farrell, D.; Deschamps, J. R.; Melinger, J. S.; Bao, G.; Mattoussi, H. Resonance Energy Transfer Between Luminescent Quantum Dots and Diverse Fluorescent Protein Acceptors. *J. Phys. Chem. C* **2009**, *113*, 18552–18561.